Received: 16 August 2022 | Revised: 1 August 2023 | Accepted: 8 August 2023

DOI: 10.1111/jmg.12746

ORIGINAL ARTICLE

Journal of METAMORPHIC GEOLOGY WILEY

Chromium in minerals as tracer of the polycyclic evolution of eclogite and related metabasite from the Pohorje Mountains, Slovenian Eastern Alps

Botao Li[1] | **Hans-Joachim Massonne**[1,2]

[1]State Key Laboratory of Geological Processes and Mineral Resources, School of Earth Sciences, China University of Geosciences, Wuhan, China

[2]Fakultät Chemie, Universität Stuttgart, Stuttgart, Germany

Correspondence
Hans-Joachim Massonne, State Key Laboratory of Geological Processes and Mineral Resources, School of Earth Sciences, Lumo Road 388, 430074, Wuhan, China.
Email: h-j.massonne@mineralogie.uni-stuttgart.de

Funding information
National Natural Science Foundation of China, Grant/Award Number: 42002068; the Most Special Fund from the State Key Laboratory of GPMR China University of Geosciences (Wuhan); 111 Project, Grant/Award Number: BP0719022

Handling Editor: Prof. Clare Warren

Abstract

Significantly different peak pressure–temperature (P–T) conditions (18–26 kbar and 630–760°C versus 29–37 kbar and 750–940°C) have previously been published for eclogite and related metabasites from the south-eastern flank of the Pohorje Mountains in Slovenia. These rocks can show a bimodal distribution of chromium in the rock-forming minerals, particularly garnet, the role of which in their metamorphic evolution is unclear. Therefore, we studied an eclogite and a related rock with clinopyroxene containing only 17 mol% jadeite + acmite (sample 18Ca35a). KαCr intensity maps of garnet particularly in sample 18Ca35a show a sharp irregular boundary between the core (Gt1) and the mantle (Gt2). Gt1 of millimetre-sized garnet in this rock is nearly Cr-free and unzoned, whereas Gt2 is of different composition (0.22 wt.% Cr_2O_3) and slightly zoned. Nearly Cr-free amphibole, (clino)zoisite, kyanite and staurolite inclusions are present in Gt1. The matrix consists of garnet and Cr-bearing clinopyroxene, (clino)zoisite and amphibole. Thermodynamic modelling suggests peak P–T conditions of 22.5 ± 2 kbar at 710 ± 25°C (Gt1) and 23 ± 2 kbar at 700 ± 25°C (Gt2) in both samples. We interpret these findings to suggest that olivine- and hornblende-bearing gabbros with some chromite experienced early metamorphism in the eclogite facies, when Gt1 formed. The rock was subsequently exhumed and cooled leading to significant garnet corrosion. A second stage of metamorphism, recognized by mappable Cr contents in garnet, led to the growth of Gt2 and other Cr-bearing minerals at the expense of chromite relics, which survived stage I. The peak P–T conditions of stage II are compatible with those previously derived by same authors and support the view that probably no ultrahigh-pressure eclogite exists in the Pohorje Mountains. We relate the two metamorphic events to the Cretaceous and Palaeogene high-pressure events recently reported from micaschists of the Pohorje Mountains.

KEYWORDS
Alpine orogeny, chromium in garnet, metabasite of the eclogite-facies, Pohorje Mountains, pressure-temperature pseudosection

1 | INTRODUCTION

The reconstruction of the pressure–temperature (P–T) evolution of high-pressure (HP) to ultrahigh-pressure (UHP) metamorphic rocks depends strongly on the composition of phengite and garnet in such rocks (Massonne, 2013). However, at temperatures above about 700°C, the common divalent cations (Ca, Fe^{2+}, Mg and Mn) in usually compositionally zoned Al-garnet tend to diffuse (e.g., Caddick et al., 2010; Carlson & Schwarze, 1997; Chakraborty & Ganguly, 1991; Dachs & Proyer, 2002; Jiang & Lasaga, 1990). This intracrystalline diffusivity leads to homogenization of such garnet over geological time scales and, thus, can complicate the decipherment of the metamorphic evolution because of the change of the original composition of a specific garnet domain. High field strength elements are characterized by low diffusion rates in garnet, but these elements usually occur only in low concentrations. Thus, it is a challenge to determine their distribution in garnet grains in thin sections over large areas and with high resolution (Rubatto et al., 2020). Chromium (which sits in the octahedral site of the garnet structure) belongs to the group of slowly diffusing cations (Carlson, 2012; Yang & Rivers, 2001); its zoning in garnet may be preserved up to temperatures of 1000°C (Massonne & O'Brien, 2003).

Variable Cr contents in X-ray maps of garnet may be used to recognize different geological processes (Rubatto et al., 2020; Spear & Kohn, 1996). For example, (1) oscillatory zoning, easily discernible in Cr maps, has been related to pulses of H_2O infiltration (Angiboust et al., 2014; Spandler et al., 2011) and (2) spiral zoning has been assigned to the rotation of garnet during growth (George et al., 2018; Martin, 2009). Here, we present another example of the applicability of different Cr contents in garnet and coexisting phases to unravel the P–T evolution of metamorphic rocks, which are metabasites from the Pohorje Mountains in northeastern Slovenia (Figure 1).

These Slovenian rocks contribute to the debate of whether UHP metamorphism occurred in the Eastern Alps (e.g., Janák, Froitzheim, et al., 2015; Janák, Uher, et al., 2015). Metabasites, mainly eclogites, from the south-eastern slope of the Pohorje Mountains were first described more than a century ago (Ippen, 1893). Their peak metamorphic evolution has been suggested at UHP conditions (peak pressures > 28 kbar; Hauzenberger et al., 2016; Janák et al., 2004; Janák, Froitzheim, et al., 2015; Janák, Uher, et al., 2015; Vrabec et al., 2012) or at HP conditions (around 22.5 kbar; Miller, Mundil, et al., 2005; Sassi et al., 2004). Our study proposes that metabasite from the same area experienced a maximum peak pressure of only about 23 kbar. Such high pressures were reached twice during different metamorphic events discernible by the Cr zonation in garnet. The derivation of the polycyclic HP metamorphism in this study supports the finding by Li, Massonne, Koller, and Zhang (2021), Li et al. (2023) that both a Late Cretaceous and a Palaeogene orogenic event affected the Pohorje Mountains. Thus, our study has major implications for the geotectonic evolution of the south-easternmost Alps.

2 | GEOLOGICAL SETTING

The Alps formed by the Cretaceous to a recent collision of the Adria plate with subducting Mesozoic and Cenozoic oceans and the European passive continental margin (Dal Piaz et al., 2003). Two HP-UHP metamorphic events occurred in the Eastern Alps in the Late Cretaceous (Eo-Alpine) and Cenozoic (Neubauer et al., 2000; Schmid et al., 2004). In addition, some metamorphic rocks of the Alpine events underwent Variscan and late Permian orogenic cycles (e.g., Schuster & Stüwe, 2008; Thöni, 2006; Thöni & Miller, 2009). Late Permian metamorphism in the Eastern Alps is commonly characterized by low peak pressures (Habler & Thöni, 2001), but high peak pressures were also reported (Hauke et al., 2019).

Traditionally, the Alps are subdivided into the Penninic, Austroalpine and Helvetic zones and the Southern Alps (Figure 1a) with the Austroalpine nappes mainly exposed in the Eastern Alps (Dal Piaz et al., 2003). The Austroalpine nappe stack can be further subdivided from bottom to top into the thrust sheets of the Lower Austroalpine, the Lower Central Austroalpine and the Upper Central Austroalpine (e.g., Hoinkes et al., 1999).

2.1 | Pohorje Mountains

The Pohorje Mountains in the southeastern Eastern Alps is related to the Central Austroalpine basement (Figure 1b). The Pohorje area consists of a nappe stack composed of three tectonic units (Hauzenberger et al., 2016). The lower Pohorje Nappe is considered part of the Lower Central Austroalpine (Janák et al., 2006) and consists of micaschist,

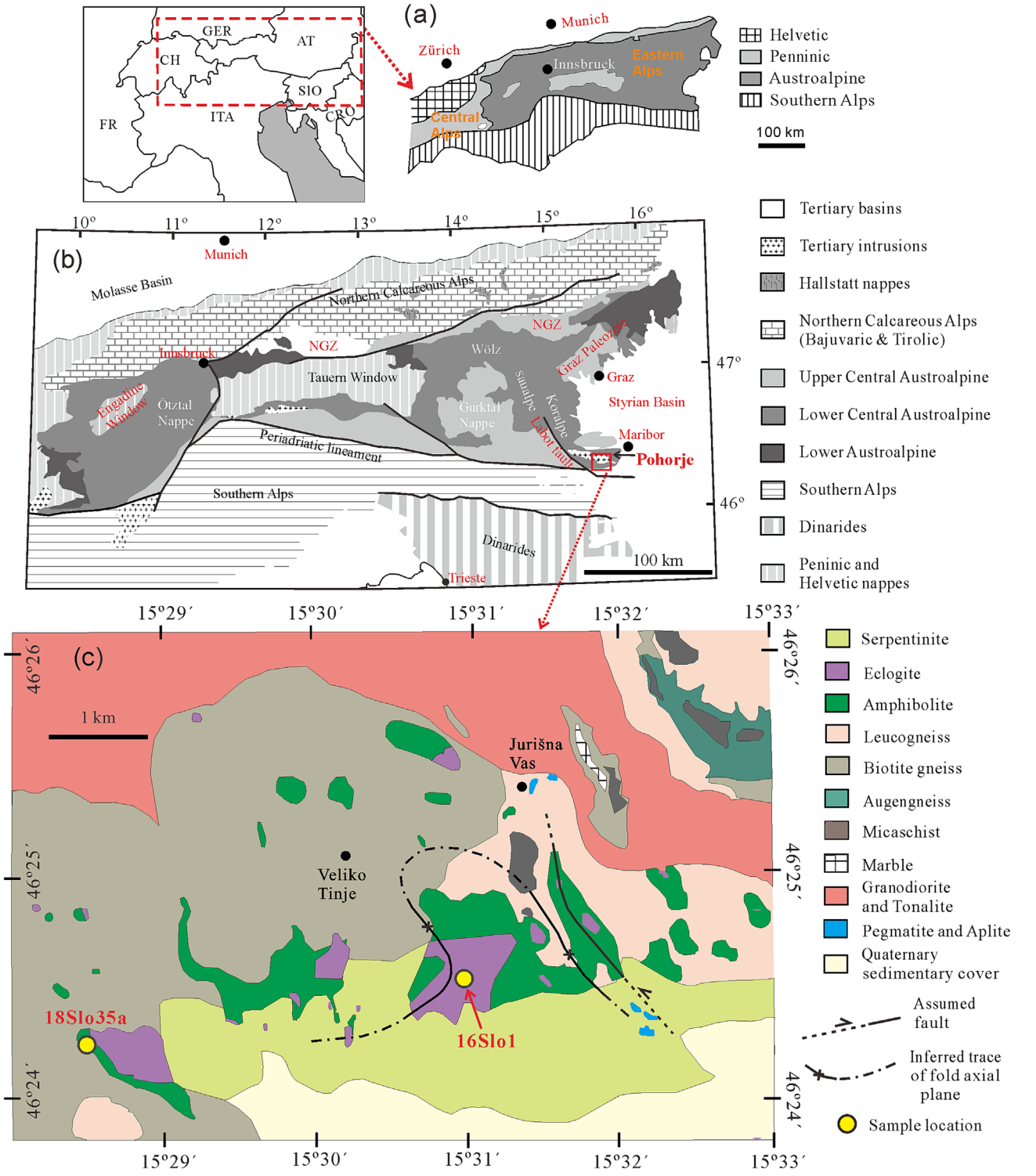

FIGURE 1 (a) Tectonic map according to Ratschbacher et al. (1989) showing the main units of the central and eastern Alps with (b) a more detailed map after Uher et al. (2014) and Sandmann et al. (2016). (c) Geological map of the southeastern Pohorje after Kirst et al. (2010) and Uher et al. (2014). Sample locations are marked by yellow spots.

gneiss and amphibolite with lenses of marble, quartzite, eclogite and ultramafic rocks (Figure 1c). Typically, the sizes of eclogite (and similar metabasite) lenses are in the dekametre range but can be up to several hundred metres in length. The Pohorje nappe is folded into an ESE–WNW-striking antiform around the Oligocene–Miocene Pohorje tonalitic–granodioritic pluton (Altherr et al., 1995; Fodor et al., 2008) and overlain by Palaeozoic slate and phyllite (middle unit) and Permo-Triassic sandstone and conglomerate (upper unit; Hauzenberger et al., 2016).

Middle and upper units represent the Upper Central Austroalpine in the Pohorje Mountains (Janák et al., 2006).

Metamorphism in the Pohorje nappe occurred during the Late Cretaceous: (1) U–Pb ages of zircon in eclogite, metapelite and orthogneiss (Miller, Mundil, et al., 2005; Janák et al., 2009; Chang et al., 2020: 89–93 Ma) (2) Sm–Nd garnet ages of eclogite (Miller, Mundil, et al., 2005: 87–95 Ma), gneiss and micaschist (Thöni, 2003: 84–95 Ma), (3) a Lu–Hf garnet age of eclogite [Thöni et al., 2008: 93.3 ± 2.8 (2σ) Ma], (4) in situ U–Th–Pb ages of monazite in metapelite determined with the electron microprobe (EMP; Krenn et al., 2009; Li, Massonne, Koller, & Zhang, 2021: 90–106 Ma) and (5) in situ U–Pb ages of monazite in metapelite obtained by laser ablation inductively coupled plasma mass spectrometry [LA-ICP-MS; Li et al., 2023: 90.62 ± 2.78 (2σ) Ma].

Despite the similarity in ages, significantly different peak P–T conditions were derived for the Pohorje metamorphic rocks (Figure 2). Studies of the metamorphic evolution of eclogites suggested conditions in the range of 18–37 kbar and 630–940°C (Hauzenberger et al., 2016; Janák et al., 2004; Janák, Uher, et al., 2015; Miller, Mundil, et al., 2005; Miller, Thöni, et al., 2005; Sassi et al., 2004; Vrabec et al., 2012; Figure 2). Miller and Konzett (2005) demonstrated that the choice of the geothermobarometric methods significantly influenced the calculated conditions. Studies of metasedimentary country rocks suggested a similar but lower-range in Late Cretaceous peak-pressure conditions between 13 and ≥35 kbar at 600–850°C (Herg & Stüwe, 2018; Hurai et al., 2010; Janák et al., 2009; Janák, Froitzheim, et al., 2015; Krenn et al., 2009; Li et al., 2023; Li, Massonne, Koller, & Zhang, 2021). Li, Massonne, Koller, and Zhang (2021) reported an additional P–T loop during the Cenozoic [between 26.2 ± 2.8 (2σ) and 47.9 ± 10.8 Ma] leading to peak pressures of 18.5–23 kbar at temperatures somewhat below 600°C. This HP event was related by these authors to the one that is more discernible in the Tauern window (Figure 1b; 17–24 kbar, ≤635°C) at 31–<45 Ma (Dachs & Proyer, 2002; Holland, 1979; Hoschek, 2004; Hoschek et al., 2010; Spear & Franz, 1986; Stöckhert et al., 1997: Thöni, 2006).

2.2 | Adjacent Koralpe–Saualpe high-pressure terrane

The HP rocks of the Koralpe–Saualpe terrane, being adjacent to the Pohorje Mountains to the northwest (Figure 1b), show similarities to those of the Pohorje Mountains and were, therefore, suggested to be part of the same deeply buried crust (Janák et al., 2004, 2009). Late Cretaceous ages (c. 85–110 Ma) were reported for metamorphic rocks of this terrane (Miller & Thöni, 1997; Thöni, 2003; Thöni & Jagoutz, 1992; Thöni & Miller, 1996), the south-eastern part of the polymetamorphic Koralpe–Wölz HP nappe system. The metamorphic history of the Koralpe–Saualpe terrane is

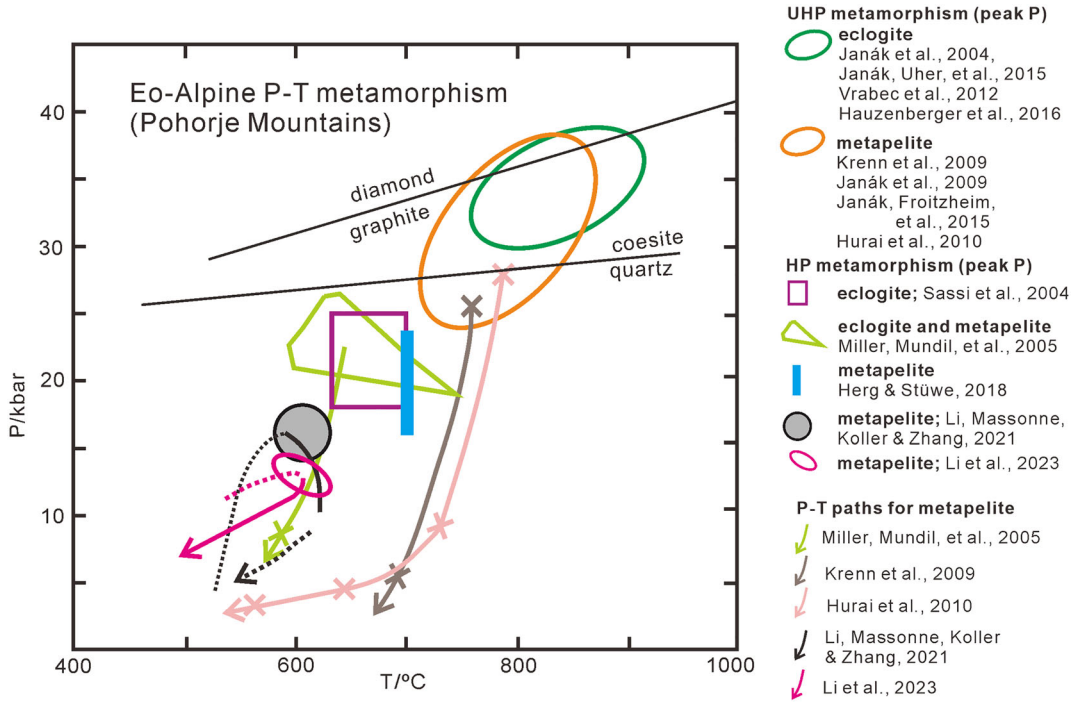

FIGURE 2 Previously reported (see legend) late cretaceous (Eo-Alpine) P–T conditions and paths for metamorphic rocks from the Pohorje Mountains, modified from Li, Massonne, Koller, and Zhang (2021).

characterized by high peak pressures recorded in both metabasites (Bruand et al., 2010; Miladinova et al., 2021; Miller, Thöni, et al., 2005; Schorn et al., 2021; Thöni et al., 2008: 18.5–23.5 kbar, 670–720°C) and metapelites (Faryad & Hoinkes, 2003; Schulz, 2017; Thöni & Miller, 1996, 2010: 12–20 kbar at 680–735°C). Herg and Stüwe (2018), Schorn and Stüwe (2016) and Tenczer and Stüwe (2003) also estimated lower peak pressures for metapelites of the Koralpe unit and the overlying Plankogel unit compared to the metabasites. Almost all P–T estimates of these authors range between 7 and 16 kbar and between 530 and 750°C. Thus, Schorn and Stüwe (2016) concluded that metapelite and eclogite experienced different early P–T evolutions with eclogite being subject to significantly deeper burial than metapelite.

HP-UHP metabasites of the Saualpe–Koralpe (–Pohorje) region of the Eastern Alps were geochemically analysed to investigate the protolith evolution (Miller et al., 1988, 2007; Miller, Mundil, et al., 2005; Miller & Thöni, 1997; Sassi et al., 2004; Thöni & Jagoutz, 1992). These studies yielded mid-ocean-ridge basalt (MORB)-type protoliths (Miller, Thöni, et al., 2005), which, according to major- and trace-element systematics, were low-Mg gabbros, derived from evolved tholeiitic magmas not significantly influenced by cumulate formation, and high-Mg–Al–Ca gabbros. The latter type, which is depleted in alkalis and shows pronounced positive Sr and Eu anomalies, is considered to represent plagioclase-rich cumulates (Miller, 1990; Sassi et al., 2004). Low Ti and high Cr (400–1,240 ng/g rock) contents in the metamorphosed high-Mg–Al–Ca gabbros are typical (Miller, Thöni, et al., 2005). The high Cr contents point to Cr-rich spinel among the cumulate minerals, which was detected in such rocks as relics (Hauzenberger et al., 2016). Occasionally, the transition from gabbro, which is mainly composed of plagioclase + clinopyroxene ± orthopyroxene ± olivine, to eclogite can be retraced (Heritsch, 1973; Thöni & Jagoutz, 1992).

2.3 | Sampling

Eclogite and country rock from the south-eastern slope of the Pohorje Mountains were sampled in 2016 and 2018. Two relatively fresh metabasites, samples 16Slo1 and 18Slo35a (Figure 1c), were selected for the detailed study after microscopic investigation and analysis of minor and major elements with X-ray fluorescence (XRF) spectrometry and preliminary EMP analyses of minerals. 16Slo1 was taken from a block north of the road from the village of Visole to Veliko Tinje in a forest area (coordinates: N46°24.544′, E15°30.972′); 18Slo35a was sampled from one of several small outcrops along the Ložnica creek (coordinates: N46°24.241′, E15°28.537′) characterized by a bank exposing a relatively homogeneous rock face overlying a several square metre-sized rock wall.

3 | METHODS

3.1 | Analytics

Textural relations of the minerals and modal mineralogy (by standard point-counting) were studied in polished thin sections (30 μm thick) of the metabasites using a polarizing microscope.

The chemical compositions of minerals were determined using a CAMECA SX100 EMP with five wavelength-dispersive spectrometers at the Institut für Anorganische Chemie, Universität Stuttgart. Concentrations of Na, K, Mg, Ca, Fe, Al, Si, Mn, Ti and Cr were measured with 15 kV accelerating voltage, 15 nA beam current and a slightly defocused beam (diameter: 3–5 μm) on a standard polished thin section. For such analyses, 20 seconds counting time per element each at the peak and on the background was applied (for analytical errors see Massonne, 2012). Zinc was additionally analysed in staurolite. Standards were minerals and pure oxides. The procedure provided by CAMECA was applied to correct the raw data. Mineral formulae of silicates were calculated from EMP analyses with the program CALCMIN (Brandelik, 2009): (1) Al+Cr+Fe+Mn+Mg+Ca +Na = 10 and Fe^{3+} = 4–Al–Cr for garnet; (2) six oxygen anions and four cations for omphacite; (3) 21 oxygen anions, 1 H_2O and Si + Ti + Al + Cr + Fe + Mn + Mg = 13 for amphibole; (4) 12.5 oxygen anions, 0.5 H_2O and Fe and Mn as only trivalent cations for (clino) zoisite; (5) 5 oxygen anions and Fe and Mn as only trivalent cations for kyanite and (6) 30 cations, 1 H_2O, and Fe and Mn as divalent cations for staurolite.

X-ray maps for Ca, Cr, Fe, Mg and Mn in garnet (and surrounding minerals) were obtained with the EMP by applying 15 kV accelerating voltage, 60 nA beam current and 100 ms counting time per step. Different step widths were used depending on the size of the scanned area. A FEI Quanta 450 FEG scanning electron microscope (SEM) connected with an energy-dispersive spectrometer (EDS) at the State Key Laboratory of Geological Processes and Mineral Resources, China University of Geosciences (CUG), Wuhan, was used to prepare back-scattered electron (BSE) images. Small inclusion minerals were identified based on analyses with the EDS.

Elemental concentrations in the bulk rock were analysed at the Institut für Mineralogie und Kristallchemie (IMK), Universität Stuttgart, with a PHILIPS PW2400 XRF spectrometer and certified geostandards. The rock slab, from which the thin sections were prepared, was

broken and ground with a tungsten carbide dish-and-puck mill. The obtained powder was fused with Spectromelt® (ratio 1:6) to prepare a glass disc from which major and minor elements were analysed. This disk was also analysed for 40 different trace elements from Sc to U by LA-ICP-MS combining a Cetac LSX-213 system, with a wavelength of 213 nm, and an AGILENT 7700 s ICP mass spectrometer at the IMK. Spot size, laser shot frequency and laser energy were 100 μm, 10 Hz (for an acquisition time of 90 s) and 50%, respectively. The transport of the ablated material to the mass spectrometer was performed in a He–Ar atmosphere (He = 300 and Ar = 800 mL/min). Standards for calibration were DLH-7 and DLH-8 glasses from the P&H Developments Ltd. Company and a NIST 612 glass. Silicon was used as an internal standard, employing the content of this element previously measured by XRF spectroscopy. For a quality check of the applied method, glass discs were analysed, which were prepared from Spectromelt® and diorite (DR-N) or zinnwaldite (ZW-C) reference standards from the Service d'Analyses des Roches et des Minéraux at Centre National de la Recherche Scientifique. For more details, the reader is referred to Massonne et al. (2022).

Trace element analyses of garnet were obtained on a 50-μm-thick polished thin section by LA-ICP-MS at the State Key Laboratory of Geological Processes and Mineral Resources, CUG, Wuhan. Laser sampling was performed using a GeoLas 2005 System coupled to an AGILENT 7500a ICP-MS instrument. Garnet was ablated using spot diameters of 44 μm, a repetition rate of 8 Hz, and a fluence of 7 J/cm^2. Helium was used as the carrier gas in the ablation cell and merged with argon behind this cell (Luo et al., 2018). Each analysis consisted of 20 s of background signal acquisition followed by 70 s of ablation. In order to avoid downhole fractionation, the signals of the last 20–30 s of the ablation were ignored. Elemental concentrations were calibrated against multiple-reference materials (BCR-2G, BIR-1G, BHVO-2G) with the 100% normalization-calibration strategy (Li et al., 2015). Standards were analysed before and after the analysis campaign and after every 8 garnet analyses (for mean results see Table S1). Off-line data calibration considering the downhole fractionation by laser ablation was performed by the ICPMSDataCal software (Liu et al., 2008). Other detailed instrumental settings and analytical techniques were outlined in Liu et al. (2008).

3.2 | Thermodynamic modelling

P–T pseudosections for samples 16Slo1 and 18Slo35a were calculated with PERPLE_X (Connolly, 2005) in the 10-component system Na–Mg–Ca–Mn–Fe–Al–Si–Ti–O–H. Two commonly used thermodynamic data sets including versions of PERPLE_X were applied to check the congruity of the obtained results (as proposed by Li, Massonne, Koller, & Zhang, 2021; Massonne & Li, 2022; Pan et al., 2020): (1) thermodynamic data set 1 (PERPLE_X version 6.6.6, data for mineral end-members by Holland & Powell, 1998, updated in 2002) was used to calculate pseudosections in the P–T range 3–28 kbar and 450–850°C; (2) thermodynamic data set 2 (PERPLE_X version 6.8.8, data for mineral end-members by Holland & Powell, 2011) was applied to a Mn-free system and the P–T range 15–28 kbar and 610–850°C. The calculated pseudosections were contoured with isopleths of various parameters such as XCa, XMg and modal content of garnet and Si pfu in amphibole. The raw curves obtained with PERPLE_X were smoothed for diagrammatic presentation (Connolly, 2005; Figures 7–9 and S1). The applied solid solution models (see Appendix A) were those reported in Massonne and Li (2022).

The bulk rock compositions for samples 16Slo1 and 18Slo35a determined by XRF were normalized to 100 wt% after adding O_2 (0.1 wt% resulting in considerable Fe^{3+} contents in the normalized bulk rock), an equivalent of Cr_2O_3 to Al_2O_3 (only 18Slo35a) and H_2O (4 wt%, Table 4) since test runs had demonstrated that the selected amount of water was sufficient to reach water-saturated conditions at the metamorphic peak. The added O_2 is equivalent to the Fe^{3+} content in the rocks estimated from the composition and mode of the minerals (see Table S2). This estimation method was also applied to obtain an effective bulk rock composition for metamorphic stage II (= formation of Gt2 and other relatively Cr-rich minerals; stage I refers to Gt1 and Cr-poor minerals). The composition resulting from the removal of Gt1 (Table S2), is very similar to that of the bulk rock composition and was ignored for further calculations. However, a pseudosection was calculated without O_2 for sample 18Slo35a, using only thermodynamic data set 1, in order to check the influence of different oxidation states of the bulk rock.

To better understand the stable appearance of a Cr-rich spinel (chromite) in metabasite, calculations in the system Cr–Na–Mg–Ca–Fe–Al–Si–O–H were performed with PERPLE_X version 6.8.8. Only the Cr, H_2O and O_2 (Fe^{3+}) contents in a selected metabasic bulk rock composition were modified (Table 4). We used the thermodynamic data set for mineral end-members by Holland and Powell (2011) and the solid solution models for clinopyroxene, garnet, orthopyroxene and spinel by Jennings and Holland (2015) containing Cr components. Though these models were calibrated by Jennings and Holland (2015) for modelling phase equilibria of mantle minerals (+ melt), we used these models to explore those of Cr-bearing minerals in metabasite. In addition, the model feldspar by Fuhrman and Lindsley (1988) for plagioclase

was applied. The P–T range of 3–28 kbar and 450–850°C was considered for the calculations.

4 | RESULTS

4.1 | Petrography and chemical compositions of minerals in sample 16Slo1

Sample 16Slo1 is a nearly equigranular eclogite (Figure 3a–c) consisting of omphacite (45 vol.% including symplectites at the omphacite margin), garnet (27 vol.%), (clino)zoisite (15 vol.%), quartz (7 vol.%) and amphibole (4 vol.% without secondary amphibole). Accessories are kyanite, rutile, sulphides and diverse secondary minerals. The latter minerals such as greenish amphibole, chlorite, and plagioclase are fine-grained and mainly occur around garnet and omphacite and in cracks through the rock. Typically, symplectites of amphibole and plagioclase with various lamella sizes (Figure 3d) surround omphacite.

Garnet grains are between 0.2 and 2 mm in size with a mean diameter of about 0.6 mm. Garnet is only weakly zoned in major elements (Figure 4) with a slight decrease of Ca from core to rim. Average molar fractions of grossular+andradite (XCa), pyrope (XMg), almandine (XFe) and spessartine (XMn) are 0.20–0.21, 0.46, 0.32 and 0.01, respectively (Table 1). A core–rim difference in Cr concentrations is visible (Figure 4b), which was used to define the garnet domains Gt1 (core) and Gt2 (mantle + rim). Average Cr_2O_3 concentrations in Gt1 and Gt2 are 0.01 wt% and 0.10 wt%, respectively, based on EMP analyses (Table 1). The former value (109 ng/g, Table S2) is confirmed by LA-ICP-MS (Table 2), whereas the Cr content determined for Gt2 (279 ng/g) is lower than analysed with the EMP possibly because ablation at garnet rims was not undertaken. Inclusions in garnet are nearly

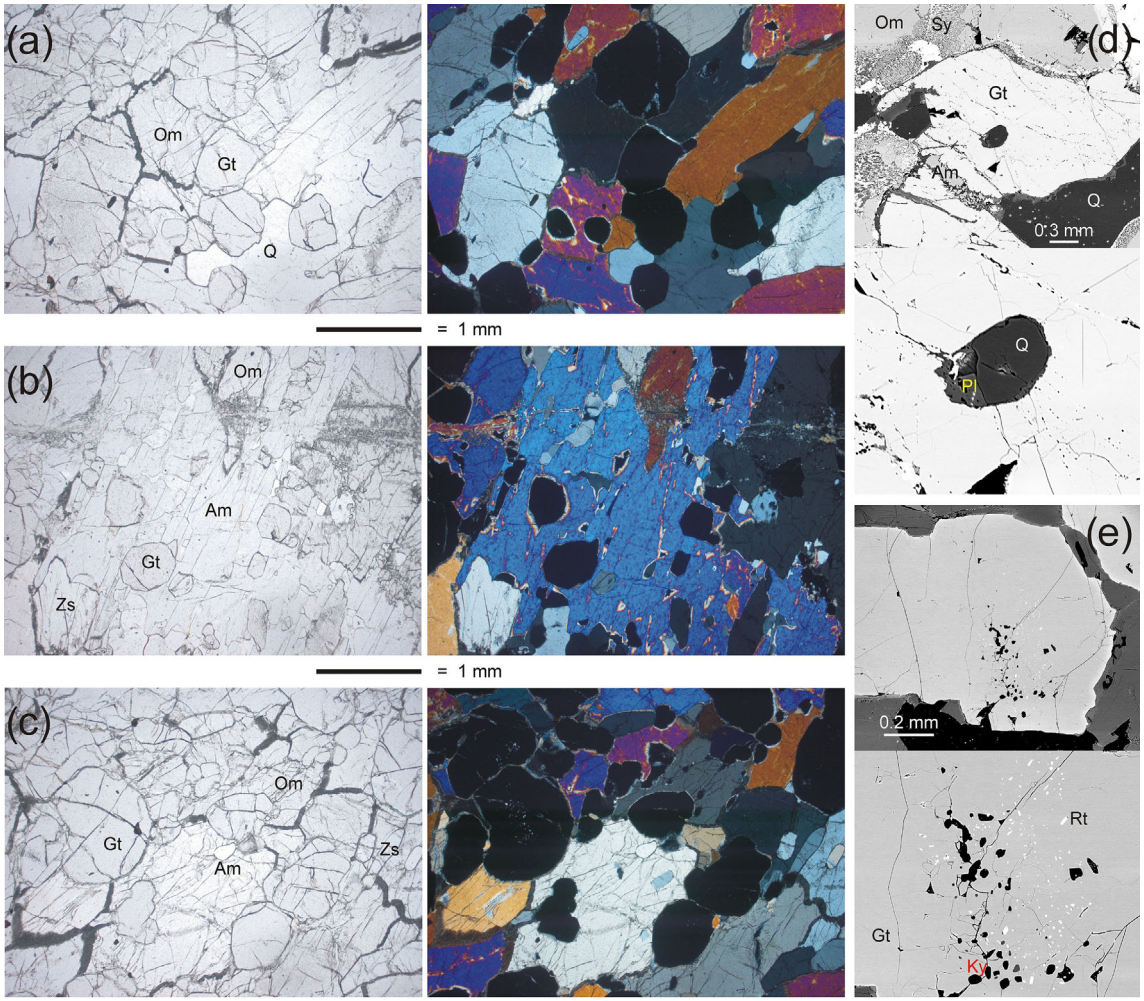

FIGURE 3 (a–c) Photomicrographs taken on a thin section of eclogite 16Slo1 under plane polarized light and crossed polarizers. (d–e) Back-scattered electron images show textural features and particularly inclusions in garnet. Abbreviations: Am = amphibole, Gt = garnet, Ky = kyanite, Om = omphacite, Pl = plagioclase, Q = quartz, Rt = rutile, Sy = symplectite, Zs = (clino)zoisite.

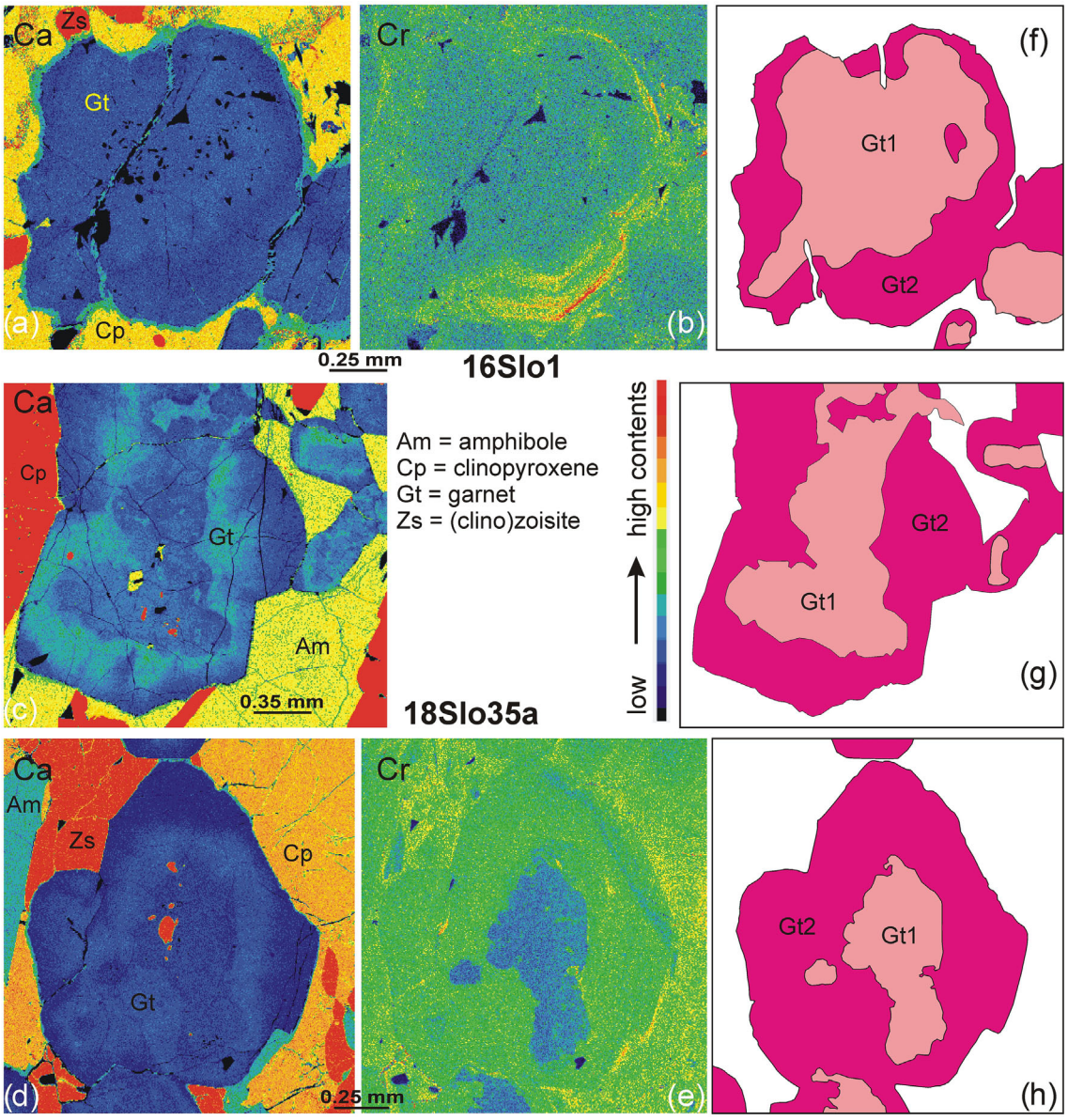

FIGURE 4 (a–e) X-ray maps of garnet in samples 16Slo1 and 18Slo35a showing the distribution of Ca and Cr. The colour scale refers to counts of specific Kα radiation per time unit. (f–h) Relatively Cr-poor Gt1 (pink) and Cr-rich Gt2 (magenta) were outlined for the three garnet grains shown in (a–e).

confined to the Gt1 domain. Usually, we found relatively large quartz grains (Figure 3d) and clusters of small kyanite or rutile grains (Figure 3c,e). Inclusions of omphacite are rare but present in Gt1.

Omphacite grains are commonly larger than garnet grains. The largest omphacite grains (up to 5 mm) contain Gt1 inclusions (Figure 3a). The EMP analyses suggest the presence of low-Cr domains (average of 0.02 wt% Cr_2O_3) in the core of large grains and as inclusion in Gt1 and relatively high-Cr (0.07 wt% Cr_2O_3) omphacite both with 30 mol% jadeite (+acmite) component (Table 1).

(Clino)zoisite (up to 2.5 mm) is a common matrix mineral and is found as inclusion in large amphibole and omphacite. The composition of (clino)zoisite is characterized by 9 mol% epidote component, $Ca_2Al_2Fe^{3+}Si_3O_{12}(OH)$. There was no discernible zoning in Cr. Analyses moderately scatter around 0.06 wt% Cr_2O_3 (Table 1).

Primary amphibole (magnesio-hornblende) with a grain size of up to 5 mm occurs in the matrix as a minor mineral. These large grains enclose garnet, omphacite, (clino)zoisite, and quartz (Figure 3b,c). The amphibole generally contains relatively high Cr concentrations (Table 1: average of 0.08 wt% Cr_2O_3, but core analyses yielded values slightly above 0.10 wt% Cr_2O_3). Concentrations of Si per formula unit (pfu) decrease from the core (6.95 Si pfu) towards the rim (6.7 Si pfu). Concentrations of Ca and Mg are around 1.55 and 3.7 pfu, respectively.

TABLE 1 Average of EMP analyses of minerals in eclogite sample 16Slo1 including their structural formulae.

Mineral	Garnet		Clinopyroxene				
Generation	Low-Cr	High-Cr	Low-Cr	High-Cr	Amphibole	(Clino)zoisite	Kyanite
n	21	26	10	12	18	10	3
SiO2 in wt%	40.64	40.54	55.20	55.09	49.73	39.46	37.12
TiO2	0.06	0.03	0.13	0.13	0.26	0.06	0.02
Al2O3	23.15	23.11	8.94	8.87	11.81	32.60	63.64
Cr2O3	0.01	0.10	0.02	0.07	0.08	0.06	0.00
Fe2O3	0.80	0.70	1.26	1.33	4.97	1.61	0.53
FeO	16.04	16.05	1.64	1.53	0.66		
MnO	0.42	0.43	0.01	0.02	0.04	0.01	0.01
MgO	12.98	13.07	11.88	11.92	17.99	0.10	0.01
CaO	8.11	7.92	18.05	17.94	10.73	25.05	0.02
Na2O	0.02	0.01	4.35	4.35	2.68	0.00	
K2O			0.00	0.01	0.24		
Total	102.23	101.96	101.49	101.26	99.19	98.94	101.35
Si	5.828	5.823	1.942	1.943	6.802	2.980	0.989
Ti	0.006	0.004	0.003	0.003	0.026	0.003	0.000
Al	3.912	3.913	0.371	0.369	1.904	2.902	1.999
Cr	0.001	0.012	0.001	0.002	0.008	0.003	0.000
Fe^{3+}	0.087	0.075	0.033	0.035	0.511	0.091	0.011
Fe^{2+}	1.923	1.929	0.048	0.045	0.076		
Mn	0.052	0.052	0.000	0.001	0.005	0.000	0.000
Mg	2.774	2.798	0.623	0.627	3.667	0.011	0.000
Ca	1.246	1.218	0.681	0.678	1.573	2.027	0.001
Na	0.006	0.003	0.297	0.298	0.711	0.001	
K			0.000	0.000	0.043		

Note: Iron in (clino)zoisite and kyanite was assumed to be trivalent, whereas Fe^{2+} and Fe^{3+} (as well as FeO and Fe_2O_3) in the other minerals were calculated as given in the text.
Abbreviation: *n*, number of analyses.

Secondary amphibole around garnet contains about 6.4 Si, 3.35 Mg and 1.7 Ca pfu.

Quartz occurs in the matrix as up to millimetre-sized grains as well as inclusions in all major and minor minerals. Rutile was rarely found as small grains up to 50 μm in the matrix. Kyanite in the clusters in garnet contains about 1 mol% $AlFe^{3+}SiO_5$ component and virtually no Cr.

4.2 | Petrography and chemical compositions of minerals in sample 18Slo35a

Sample 18Slo35a, looking macroscopically like an eclogite, is a clinopyroxene–garnet–amphibole–(clino)zoisite fels consisting of clinopyroxene (33–35 vol.%), garnet (32–34 vol.%), amphibole (17–19 vol.%) and (clino)zoisite (13–15 vol.%) with accessory kyanite, staurolite, rutile, sulphides and very fine-grained secondary minerals along cracks and in symplectites at clinopyroxene rims.

Garnet grains are between 0.3 and 2 mm in size with a mean diameter of about 0.8 mm. X-ray maps of several grains show that garnet is compositionally zoned in Cr (Figure 4). A poorly zoned low-Cr core domain (Gt1), which according to X-ray maps of Ca and Cr forms about 5 vol.% (Table S2), contains mean Cr and Cr_2O_3 contents of 233 ng/g (LA-ICP-MS: Table 2, Table S2) and 0.03 wt% (EMP, Table 3), respectively. The average composition of Gt1 is characterized by XMn = 0.005, XCa = 0.185, XMg = 0.645 and XFe = 0.165. However, XCa can be somewhat variable (see the blurred Gt1 domain in the Ca map of Figure 4c) ranging between 0.145 and 0.205 (Figure 5). The mantle domain (Gt2) shows relatively

TABLE 2 Mean trace-element contents (with standard deviation) in garnet determined by combined laser ablation and ICP-MS.

Sample	**16Slo-1**		**18Slo-35a**	
Garnet domain	**Gt1 = Cr-poor**	**Gt2 = Cr-rich**	**Gt1 = Cr-poor**	**Gt2 = Cr-rich**
n	**12**	**7**	**14**	**2**
P in ng/g	163 ± 41	129 ± 24	195 ± 45	142 ± 62
Sc	62 ± 9	61 ± 9	33 ± 18	65 ± 1
Ti	247 ± 78	277 ± 93	170 ± 108	113 ± 12
V	40 ± 9	42 ± 4	9.1 ± 1.2	12 ± 1
Cr	109 ± 42	279 ± 66	233 ± 94	2,215 ± 704
Co	61 ± 2	60 ± 2	69 ± 9	61 ± 4
Zn	66 ± 5	59 ± 5	27 ± 5	31 ± 6
Ga	4.3 ± 0.6	4.2 ± 0.8	3.3 ± 1.8	2.5 ± 0.2
Y	15.4 ± 5.3	16.3 ± 4.4	7.9 ± 2.9	4. 9 ± 0.1
Dy	1.52 ± 0.55	1.68 ± 0.15	1.13 ± 0.72	0.34 ± 0.14
Ho	0.56 ± 0.22	0.62 ± 0.20	0.32 ± 0.15	0.17 ± 0.08
Er	2.03 ± 0.75	2.07 ± 0.75	0.81 ± 0.20	0.63 ± 0.02
Tm	0.28 ± 0.10	0.31 ± 0.09	0.11 ± 0.03	0.15 ± 0.01
Yb	1.92 ± 0.72	2.13 ± 0.84	0.64 ± 0.28	0.88 ± 0.06
Lu	0.25 ± 0.09	0.29 ± 0.12	0.07 ± 0.03	0.12 ± 0.01

Abbreviation: *n*, number of analyses.

high Cr concentrations (mean values of 2215 ng/g Cr and 0.22 wt% Cr_2O_3) with sharp boundaries to Gt1 in Cr maps (e.g., Figure 4e) and systematically decreasing XCa from 0.23 near Gt1 to 0.17 at the rim (Figures 4c,d and 5). Such sharp boundaries are not discernible in Mg and Fe maps (not shown). The average major element composition of Gt2 is similar to that of Gt1: XMn = 0.005, XCa = 0.20, XMg = 0.635 and XFe = 0.16. Abundant inclusions were observed in the Gt1 domain including clusters of (clino) zoisite grains and small kyanite grains (Figure 6f) similar to those noted in sample 16Slo1. Polyphase inclusions mostly consisting of amphibole and staurolite (Figure 6e,h) with some kyanite (Figure 6i) are common. Clinopyroxene was found as an inclusion in Gt2 (Figure 6g).

In contrast to sample 16Slo1, only one generation of clinopyroxene (c. 17 mol% jadeite + acmite) with relatively high Cr_2O_3 contents (0.27 wt.%) was detected. This clinopyroxene mainly occurs in elongated, slightly oriented, and millimetre-sized crystals which can be as long as 8 mm. In such large clinopyroxene, millimetre-sized amphibole can be included (Figure 6c,d).

Primary amphibole (magnesio-hornblende) forms elongated, slightly oriented, and up to 5-mm-sized grains, which may include garnet, (clino)zoisite, and clinopyroxene (Figure 6a,b). The chemical composition is characterized by average Si, Ca and Mg contents of 7.09, 1.73 and 4.25 pfu, respectively, and relatively high Cr concentrations (Table 3: average of 0.29 wt% Cr_2O_3, with core analyses up to 0.4 wt% Cr_2O_3). Tschermakite amphibole in the polyphase inclusions in garnet is poor in Cr (0.04 wt% Cr_2O_3) and low in Si (around 6.2 pfu, average Ca and Mg contents: 1.71 and 4.00 pfu). A single inclusion in garnet was found with an intermediate composition between Cr-poor and Cr-rich amphibole (e.g., 0.15 wt% Cr_2O_3 as the average of three analyses, see Table 3). A third generation of amphibole is occasionally present around garnet rims (Figure 6j). The Si, Ca and Mg contents of this late generation (tschermakite to magnesio-hornblende) are around 6.5, 1.75 and 3.95 pfu, respectively. Concentrations of Cr are variable (0.05–0.31 wt% Cr_2O_3).

(Clino)zoisite is another major matrix mineral with grain sizes up to 1 mm. It commonly forms millimetre-sized aggregates of several moderately oriented grains (Figure 6c,d). Two generations were recognized based on the Cr concentrations. Small (clino)zoisite grains included in garnet and other minerals are low in Cr (mean: 0.07 wt% Cr_2O_3, Table 3) and contain 7–8 mol% epidote. Matrix (clino)zoisite is characterized by high Cr concentrations (around 0.31 wt% Cr_2O_3) and 6–7 mol% epidote (Table 3).

All analysed kyanite and staurolite, occurring only as inclusions in garnet, are nearly free of Cr (Table 3). Mg-rich staurolite contains 0.03 Zn pfu on average (Table 3). Rutile grains in the matrix are rare and small; tiny rutile grains are included in garnet.

TABLE 3 Averaged EMP analyses of minerals in garnet clinopyroxenite sample 18Slo35a including their structural formulae.

	Garnet (Gt)			Amphibole			(Clino)zoisite			
Mineral Generation	**Gt1: low-Cr**	**Gt2: high-Cr**	**Clinopyroxene**	**Low-Cr**	**High-Cr**	**Incl. in Gt**	**Low-Cr**	**High-Cr**	**Kyanite**	**Staurolite**
n	68	90	23	15	12	3	10	9	5	10
SiO_2 in wt%	41.68	41.62	54.72	45.60	52.09	48.90	39.41	39.30	36.79	28.82
TiO_2	0.01	0.02	0.10	0.11	0.18	0.25	0.17*	0.05	0.01	0.07
Al_2O_3	23.82	23.58	5.77	16.20	8.74	13.24	32.89	32.48	63.49	58.10
Cr_2O_3	0.03	0.22	0.27	0.04	0.29	0.15	0.07	0.31	0.03	0.05
Fe_2O_3	0.74	0.80	1.18	2.85	2.08	2.27	1.29	1.14	0.45	
FeO	8.36	8.23	0.15	0.00	0.00	0.00				3.94
MnO	0.24	0.25	0.02	0.02	0.01	0.01	0.01	0.02	0.01	0.04
ZnO										0.17
MgO	18.66	18.26	14.93	18.99	20.92	19.84	0.11	0.10	0.02	7.81
CaO	7.42	7.95	21.56	12.33	11.88	11.82	25.10	25.18	0.06*	
Na_2O	0.01	0.01	2.44	2.24	1.79	2.06	0.00	0.00	0.01	
K_2O			0.00	0.05	0.11	0.15				
Total	100.96	100.94	101.14	98.44	98.09	98.68	99.06	98.60	100.86	98.99
Si	5.819	5.826	1.938	6.221	7.089	6.615	2.971	2.978	0.984	7.688
Ti	0.001	0.002	0.003	0.011	0.019	0.026	0.010	0.003	0.000	0.014
Al	3.919	3.892	0.241	2.606	1.402	2.111	2.922	2.902	2.003	18.263
Cr	0.003	0.025	0.008	0.004	0.031	0.016	0.004	0.018	0.001	0.011
Fe^{3+}	0.078	0.084	0.031	0.292	0.213	0.231	0.073	0.065	0.009	
Fe^{2+}	0.975	0.964	0.004	0.000	0.000	0.000				0.878
Mn	0.028	0.029	0.001	0.003	0.002	0.001	0.001	0.001	0.000	0.008
Zn										0.034
Mg	3.884	3.811	0.788	3.863	4.245	4.001	0.012	0.012	0.001	3.103
Ca	1.110	1.193	0.818	1.802	1.732	1.713	2.028	2.045	0.002	
Na	0.002	0.002	0.168	0.593	0.473	0.539	0.000	0.001	0.000	
K			0.000	0.008	0.020	0.026				

Note: Iron in (clino)zoisite and kyanite was assumed to be trivalent and in staurolite to be divalent, whereas Fe^{2+} and Fe^{3+} (as well as FeO and Fe_2O_3) in the other minerals were calculated as given in the text.

Abbreviation: *, too high contents as the analysed minerals were small inclusions in other minerals (e.g., three analyses of low-Cr (clino) zoisite included in rutile were effected by FeKα radiation causing fluorescence of TiKα radition in rutile); Incl., inclusion; *n*, number of analyses.

4.3 | Bulk rock geochemistry

The contents of major and minor elements in the two selected samples, determined with XRF, are given in Table 4. The bulk rock compositions of samples 16Slo1 and 18Slo35a were also estimated using the average mineral compositions in Tables S2 and 4 and the mineral modes mentioned in the previous sections. The calculation procedure is presented in Table S2 and the results (Table 4) are within the analytical error of the XRF results.

The LA-ICP-MS results from sample 18Slo35a (Table S3) suggest relatively low trace-element concentrations. The rare-earth elements (REE) are in the range of chondrite values (Boynton, 1984; McDonough & Sun, 1995). However, Eu and Sr show clear positive anomalies ($Eu/Eu^* = 2.0$; $Sr_N/[Ce_N{*}Nd_N]^{0.5} = 11$).

4.4 | Modelling results

The calculated P–T pseudosections for the studied samples show typical mineral assemblages for HP metabasites. At P–T conditions of the eclogite facies, most assemblage fields in the pseudosections calculated for the bulk rock composition of 18Slo35a are without quartz

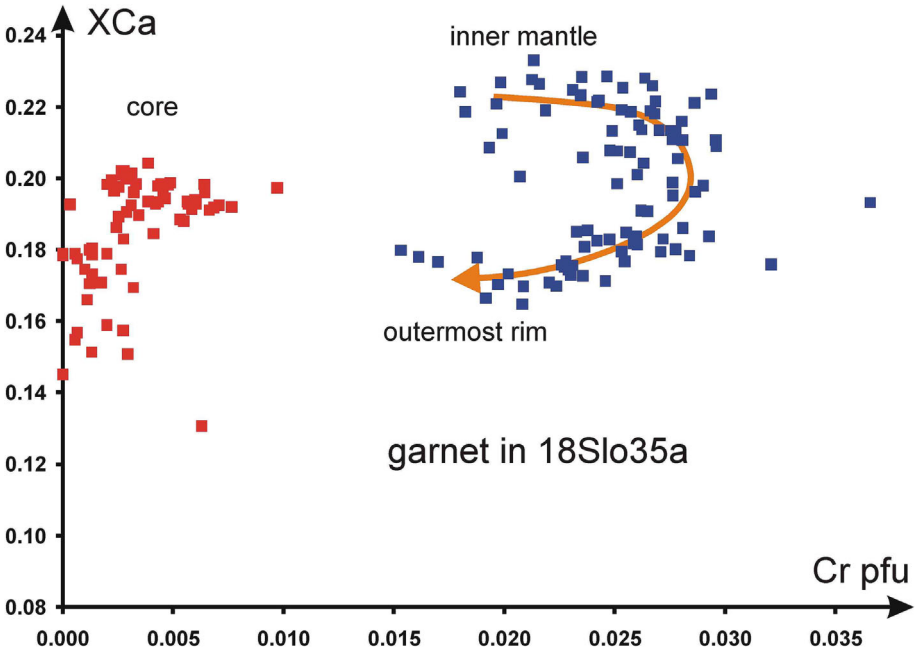

FIGURE 5 Molar fraction of grossular + andradite (XCa) versus Cr per formula unit (pfu) in garnet analysed in sample 18Slo35a. The red symbols refer to the Gt1 domain (core). Analyses of the relatively Cr-rich rim (Gt2) are marked by blue symbols. The orange line shows the chemical trend from the Gt1-Gt2 boundary towards the rim of Gt2.

(Figures 7a and 8a), whereas quartz occurs in the assemblage fields for 16Slo1 (not shown here) except at high pressures (>22 kbar) and temperatures below 650°C. The increase of the modal content and XMg (Figure 7b,c) and the decrease of XCa in garnet of the eclogite facies with rising temperature is also a common phenomenon reported in many publications on eclogite dealing with the here presented type of thermodynamic modelling.

4.4.1 | P–T conditions determined with thermodynamic data set 1

Modal content (rather for stage II), XMg, and XCa of garnet and, if applicable, the Si content in amphibole were used to constrain the P–T conditions under which the observed minerals were in equilibrium. For the uncertainties of these conditions, we assumed about ±10% of the quoted pressure and ±5% of the derived temperature. Smaller or larger uncertainties were also given depending on the proximity of the considered isopleths (Li et al., 2017). We determined the following conditions using thermodynamic data set 1: (1) 22 ± 2 kbar at 710 ± 35°C for 16Slo1 (Figure S1) with Si in the core of large amphibole (6.95 pfu) not fitting the pressure peak, (2) 23 ± 2.5 kbar at 700 ± 25°C for stage I (Gt1 formation, Figure 7d) experienced by 18Slo35a and (3) 23 ± 2.5 kbar at 730 ± 45°C for stage I (Figure 9a) in a reduced system (no Fe^{3+}) of 18Slo35a. For stage II (Gt2 formation) in this reduced system, slightly higher pressures and lower temperatures resulted (24 ± 2 kbar at 700 ± 20°C, Figure 9b). Considering that both rocks studied were subjected to the same metamorphic evolution, we suggest 22.5 ± 2 kbar at 710 ± 25°C as the most probable P–T conditions for stage I and nearly the same conditions (23 ± 2 kbar at 700 ± 25°C) for stage II.

For sample 16Slo1, the calculated mineral assemblages contain garnet, omphacite, kyanite, quartz, rutile and ±amphibole at the determined P–T conditions of both stage I and stage II (Table S4). These assemblages include the observed minerals for stage I (low-Cr minerals: Gt1, omphacite, amphibole, rutile and quartz as well as kyanite as inclusion in Gt1) and stage II (high-Cr minerals: Gt2 and omphacite). The lack of (clino)zoisite in the calculation result of Table S4 is discussed in Section 5.2. For the oxidized (Figure 7a) and non-oxidized 18Slo35a compositions, the calculated mineral assemblages at the determined P–T conditions of stage I and stage II are the same and contain amphibole, clinopyroxene, garnet, rutile, ±kyanite, ±(clino)zoisite, ±talc and ±chlorite (Table S5). Excepting staurolite (found to be included in Gt1), the calculated mineral assemblages include the observed minerals related to stage I (low-Cr minerals: Gt1, (clino)zoisite and inclusions in Gt1: kyanite, rutile and amphibole) and stage II (rutile + high-Cr minerals: Gt2, amphibole, (clino)zoisite and clinopyroxene).

4.4.2 | P–T conditions determined with thermodynamic data set 2

P–T conditions of 16.5 ± 1.5 kbar at 720 ± 20°C were estimated for stage I in 18Slo35a (oxidized composition

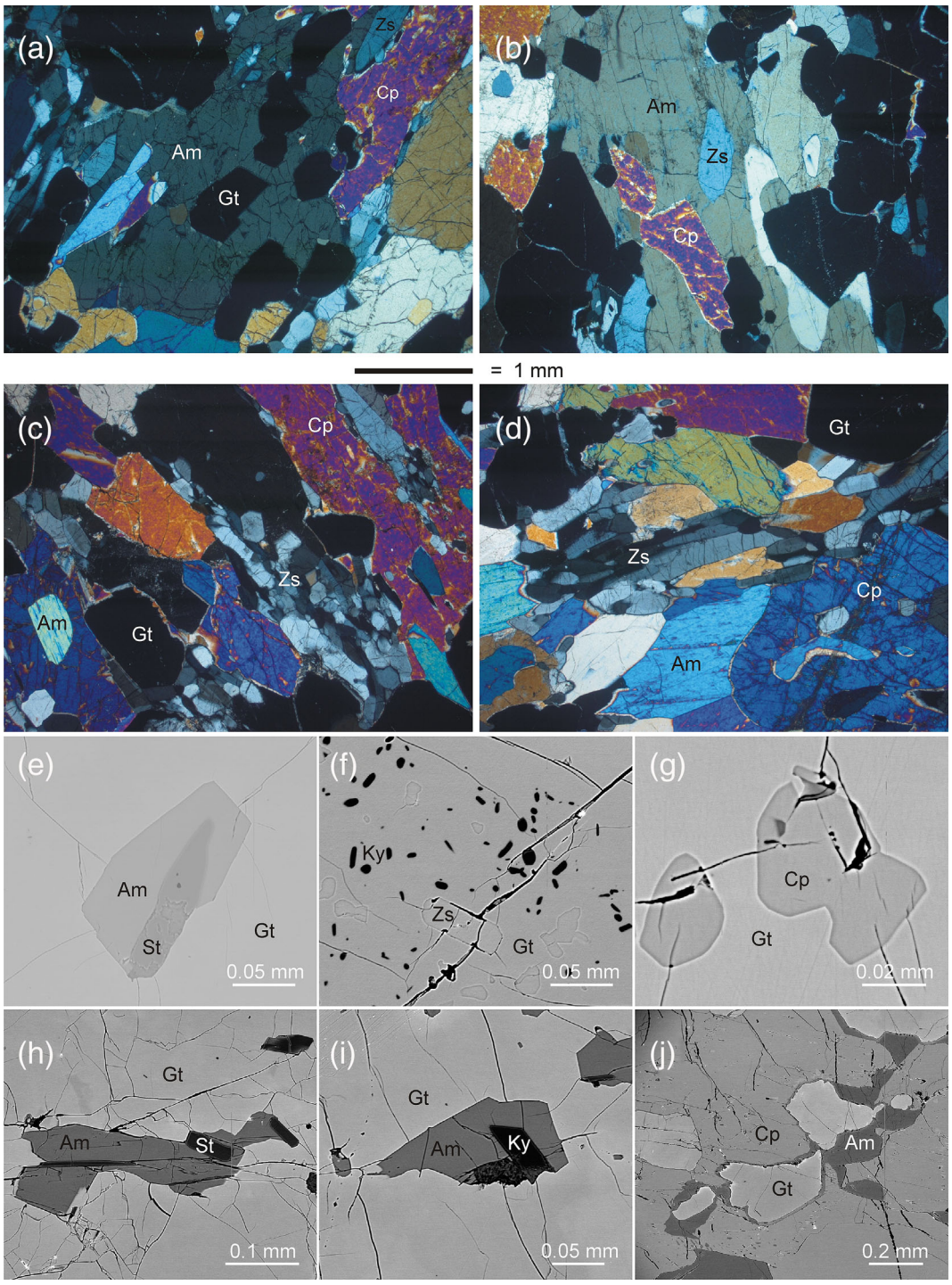

FIGURE 6 (a–d) Photomicrographs taken on a thin section of garnet clinopyroxenite 18Slo35a under crossed polarizers. (e–i) Back-scattered electron (BSE) images exhibit inclusions in garnet. (j) BSE image shows amphibole that has marginally replaced garnet. Abbreviations as in Figure 3 and Cp = clinopyroxene, St = staurolite.

without MnO) using thermodynamic data set 2 (Figure 8b). For stage II, nearly the same P–T conditions as for stage I were deduced considering errors, but somewhat higher pressures (c. 1 kbar) and lower temperatures (c. 10°C) than estimated for stage I are most likely (see the centre of the P–T ellipsis in Figure 8b). The calculated mineral assemblages (Table S6) are clinopyroxene, garnet, (clino)zoisite, ±amphibole, ±chlorite, ±kyanite, ±rutile, ±talc and ±chlorite for stage I and stage II. The consistency between calculated mineral assemblages and observed minerals is identical to the above results using thermodynamic data set 1.

TABLE 4 Bulk rock compositions based on XRF analyses and estimates presented in detail in Table S2.

				18Slo35a											
		Table S2			Table S2		PERPLE_X								
	16Slo1 XRF	Bulk rock	PERPLE_X Oxid.	XRF	Bulk rock	Eff. Bulk-r.	No Fe^{3+}	Oxid.	Cr-rich metabasite						
SiO_2 in wt.%	49.28	49.77	47.79	46.63	46.95	47.42	45.40	45.40	53.00	53.00	53.00	53.00	53.00	53.00	53.00
TiO_2	0.36	0.34	0.35	0.11	0.14	0.15	0.01	0.10							
Al_2O_3	16.28	16.15	15.79	16.86	16.73	16.35	16.57	16.57	15.00	15.00	14.00	14.00	13.00	12.00	12.00
Cr_2O_3		0.05		0.24	0.24	0.25			1.00	1.00	2.00	2.00	3.00	4.00	4.00
Fe_2O_3		1.21			1.19	1.22									
FeO	6.86	5.94	6.65	4.50	3.29	2.99	4.38	4.38	10.00	10.00	10.00	10.00	10.00	10.00	10.00
MnO	0.14	0.15	0.14	0.10	0.11	0.10	0.09	0.09							
MgO	10.03	10.18	9.72	15.05	15.50	15.35	14.65	14.65	7.00	7.00	7.00	7.00	7.00	7.00	7.00
CaO	13.92	14.18	13.50	14.14	14.75	15.25	13.77	13.77	10.00	10.00	10.00	10.00	10.00	10.00	10.00
Na_2O	2.02	2.03	1.96	0.97	1.10	1.18	0.94	0.94	4.00	4.00	4.00	4.00	4.00	4.00	4.00
K_2O	0.01			0.04											
P_2O_5	0.00			0.00											
H_2O			4.00				4.00	4.00				0.50			
O_2			0.10					0.10		0.10			0.10		0.20
SUM	98.91	100.00		98.63	100.00	100.00	99.81	100.00	100.00	100.10	100.00	100.50	100.10	100.00	100.20
PERPLE_X composition used in Figure:			S1				8	6, 7	9	9	9	9	9	9	9

Note: In addition, bulk rock compositions for calculations with PERPLE_X (see text) are given for samples 16Slo1 and 18Slo35a and a hypothetical Cr-rich metabasite that was used to decipher the upper pressure stability of chromite in this rock type.

Abbreviations: Eff., effective; Oxid., oxidized.

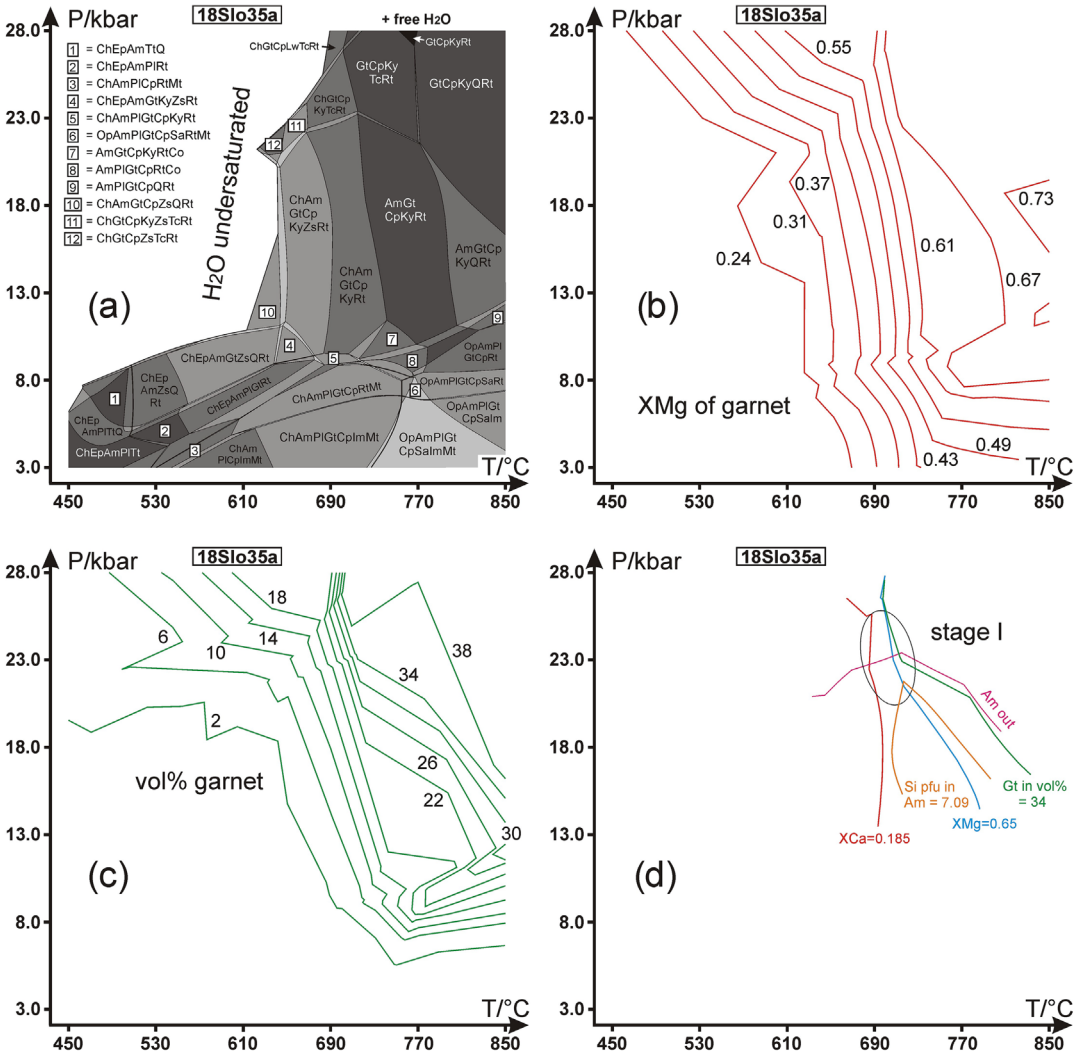

FIGURE 7 (a) Pseudosection calculated with thermodynamic data set 1 for the oxidized bulk rock composition of sample 18Slo35a (Table 4). Most fields are labelled except the very small ones. Different grey tones refer to the variance of the corresponding mineral assemblage (darker tones have a higher variance). Am, amphibole; Ch, chlorite; Cp, clinopyroxene; Ep, epidote; Gt, garnet; Im, ilmenite; Ky, kyanite; Lw, lawsonite; Mt, magnetite; Op, orthopyroxene; Pl, plagioclase; Q, quartz; Rt, rutile; Sa, sapphirine; Tc, talc; Tt, titanite; Zs, (clino)zoisite. (b–c) Contouring of the pseudosection in (a) with isopleths for XMg and modal content (vol.%) of garnet. (d) Estimation of the P–T conditions of stage I (ellipsis, assemblage of Cr-poor minerals) considering the amphibole-out curve and relevant parameters for garnet and amphibole.

4.4.3 | Cr-rich metabasite

The thermodynamic modelling to gain access to the upper pressure limit of Cr-rich spinel was performed with the seven bulk rock compositions for Cr-rich metabasite given in Table 4. The results presented in Figure 10 demonstrate that this limit increases with rising Cr_2O_3 content in the bulk rock. However, eskolaite appears at 3 and 4 wt% Cr_2O_3 and signalizes Cr saturation at the lower temperatures of the selected P–T range. The addition of H_2O has almost no influence on the upper pressure limit, whereas oxidizing conditions (Fe^{3+} contents by addition of O_2) stabilize Cr-rich spinel towards clearly higher pressures.

5 | DISCUSSION

5.1 | Protolith nature

We compared the geochemical signatures reported for HP-UHP metabasites from the Saualpe–Koralpe–Pohorje area of the Eastern Alps (see Section 2.2) with those of eclogite 16Slo1 and metabasite 18Slo35a (Tables 4 and S3) in order to define the protoliths of the rocks studied here. Miller, Mundil, et al. (2005) suggested that kyanite-rich eclogites from the Pohorje Mountains were derived from plagioclase-rich gabbroic cumulates. Although sample 18Slo35a contains kyanite only as accessory, this rock fulfils the chemical criteria for such cumulates.

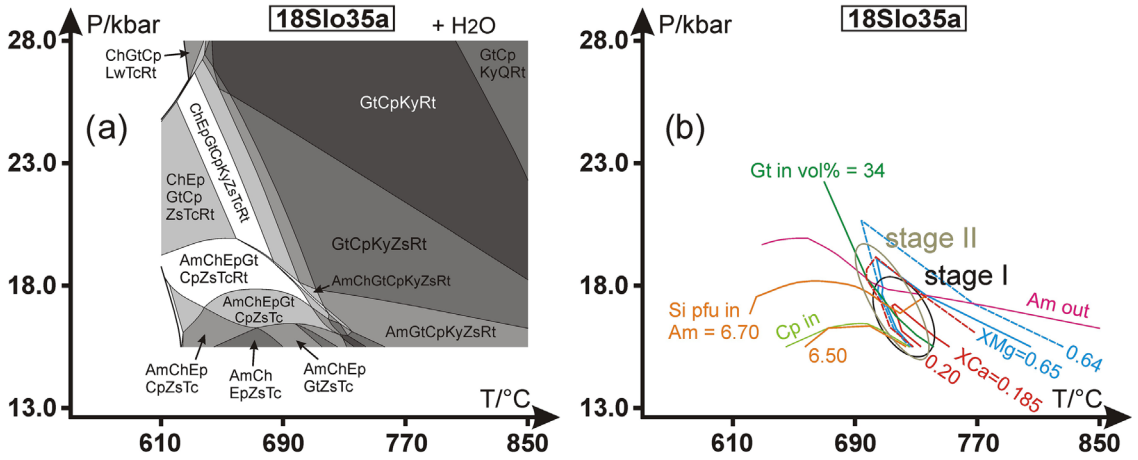

FIGURE 8 (a) Pseudosection calculated with thermodynamic data set 2 for the oxidized bulk rock composition of sample 18Slo35a (Table 4). Most fields are labelled except the very small ones. Abbreviations as in Figure 7. (b) Estimation of the P–T conditions of stages I (black ellipsis, assemblage of Cr-poor minerals) and II (olive ellipsis, assemblage of relatively Cr-rich minerals) considering the amphibole-out and clinopyroxene-in curves as well as relevant parameters for garnet (broken for Gt2) and amphibole.

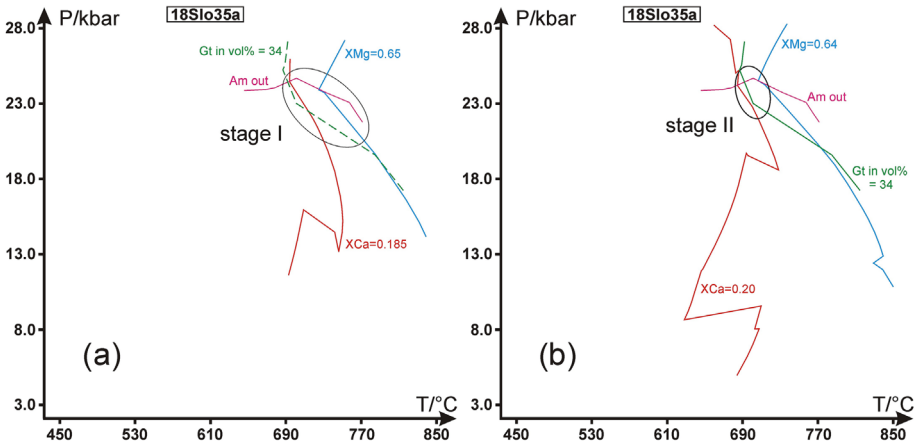

FIGURE 9 Estimation of P–T conditions considering thermodynamic data set 1 and the Fe^{3+}-free bulk rock composition of sample 18Slo35a (Table 4). (a) Ellipsis shows the most probable P–T range for metamorphism at stage I (assemblage of Cr-poor minerals) considering the amphibole-out curve and relevant parameters for garnet. (b) as (a) but for stage II (assemblage of Cr-bearing minerals).

These criteria are (1) unusually high Mg and Ca contents (18Slo35a: >14 wt% CaO, >15 wt% MgO, Table 4) compared to normal eclogites and, thus, their protoliths; (2) relatively low Ti (<0.2 wt% TiO_2) and high Cr (0.24 wt % Cr_2O_3) concentrations and (3) pronounced positive Eu (2.0) and Sr (11) anomalies (e.g., Sassi et al., 2004). Quartz-rich eclogites from the Pohorje Mountains such as 16Slo1 (7 vol.% quartz) should be less fractionated basic igneous rocks following Miller, Mundil, et al. (2005). However, we also noted the gabbroic cumulate character by elevated Mg and Ca contents (16Slo1: ≥14 wt% CaO, >10 wt% MgO, Table 4) and low Ti (c. 0.35 wt% TiO_2) and elevated Cr (c. 0.05 wt% Cr_2O_3) concentrations. In addition, the contents of REE in garnet from both studied samples (Table S2) show similar values, which are lower than those in garnet from a quartz-rich eclogite of the Pohorje Mountains studied by Miller, Mundil, et al. (2005). This could also be the result of the cumulate character of the protoliths of the rocks studied here as typical of Ti-poor eclogites from the Saualpe–Koralpe–Pohorje area (Miller et al., 1988; Miller, Mundil, et al., 2005; Miller & Thöni, 1997; Sassi et al., 2004).

5.2 | Pressure–temperature conditions

The calculated pseudosections were used to constrain the P–T conditions of the formation of Gt1 (metamorphic stage I) and Gt2 (stage II). We obtained peak pressures somewhat above (thermodynamic data set 1: 22–24 kbar) or below (data set 2: around 17 kbar) 20 kbar and peak temperatures in the range of 680–740°C for both stages. These temperatures are too low to have led to significant changes in the original compositions by intracrystalline diffusion in the millimetre-sized garnet grains (e.g., Li, Massonne, Hartmann, et al., 2021). As XMg of Gt1 and

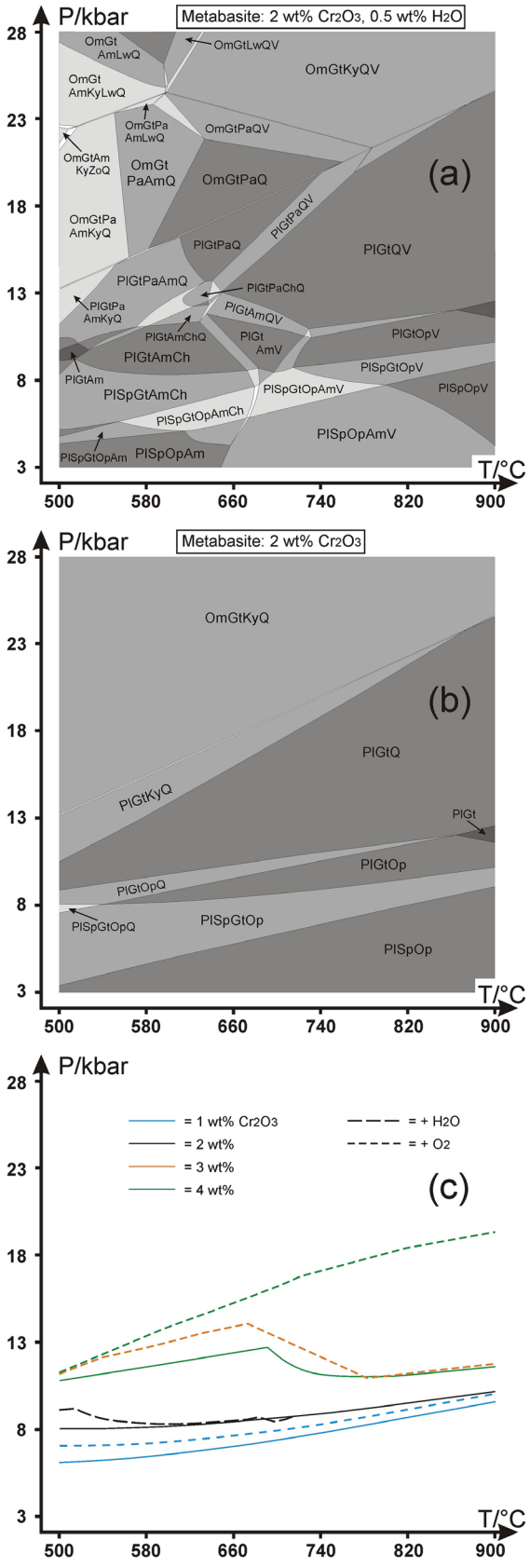

Gt2 are virtually identical, diffusion of Mg, considered as the fastest diffusing major divalent cation in garnet (e.g., Carlson, 2006; Li et al., 2018; Perchuk et al., 2009), may also be ignored. However, an extremely long residence (probably >>100 Ma, see, e.g., Massonne & Li, 2020, for millimetre-sized garnet) of the studied rocks at temperatures around 700°C could have resulted in nearly complete Mg homogenization of a previously growth-zoned garnet. But such long residence times can be ruled out because of the relatively sharp boundaries between Gt1 and Gt2 shown in Ca maps (e.g., Figure 4c). Even under the assumption of small changes of XMg compared to the originally grown garnet, the derived temperatures would not substantially change due to the minor temperature differences of relevant isopleths. For example, for sample 18Slo35a and XMg = 0.55 and 0.61, this difference is less than 15°C at pressures around 20 kbar (see Figure 7b).

At stage I, the Cr-poor garnet core (Gt1) very likely coexisted with other Cr-poor silicates and, possibly, additional inclusion minerals in Gt1. Such silicates and inclusion minerals were omphacite, kyanite, rutile, and quartz in eclogite 16Slo1 and rutile, amphibole, kyanite, staurolite and (clino)zoisite in metabasite 18Slo35a. Clusters of either small kyanite or tiny rutile grains (Figure 3e) might be residues of an Al-rich mineral (plagioclase?) or a Ti-bearing mineral (amphibole?), but these precursor minerals might be rather pre-stage I minerals. The thermodynamic modelling (thermodynamic data set 1) suggests the observed minerals included in 16Slo1 Gt1 (omphacite+kyanite+rutile+quartz) were part of the assemblage at the P–T conditions derived for stage I (22.5 kbar, 710°C, Table S4). However, it cannot be excluded that the Cr-poor silicates included in Gt1 could have formed before Gt1 (e.g., at high-pressure amphibolite–facies conditions).

For 18Slo35a, the Gt1 inclusion minerals (amphibole and kyanite) were calculated to coexist in the P–T range of stage I (thermodynamic data set 1, Figure 7), whereas (clino)zoisite and staurolite are lacking (Table S5). The P–T fields of assemblages with (clino)zoisite are limited to temperatures somewhat below 710°C (Figure 7a). This mineral was taken as pure phase in the pseudosection calculations with thermodynamic data set 1 also for the oxidized bulk rock composition (Table 4), but the

FIGURE 10 (a) P–T pseudosection calculated for a metabasite with 2 wt% Cr_2O_3 in the bulk rock composition and some H_2O (Table 4). (b) Calculation as for (a) but at dry conditions. (c) P–T position of the upper pressure limit for Cr-rich spinel calculated for seven different metabasic bulk rock compositions (Table 4). Abbreviations as in Figure 7 and Pa, paragonite; Sp, spinel; V, H_2O vapour.

limit of this phase would be shifted to higher temperatures for lower activities of endmember zoisite owing to 7–9 mol% epidote component in (clino)zoisite (Tables 1 and 3) of the rocks studied. By contrast, the calculation results for sample 18Slo35a and stages 1 and 2 using thermodynamic data set 2 yielded considerable amounts of (clino)zoisite at the deduced P–T conditions of 16.5–17.5 kbar and 710–720°C (Table S6).

The Cr-poor amphibole in 18Slo35a is low in Si (6.22 pfu in the representative amphibole analysis of Table 3) and must have been formed at considerably lower pressures than those of the P–T area for stage I (or lower temperatures), because the calculated Si in amphibole is already above 7 pfu (Figure 7d) at the pressure of stage I ($P > 21$ kbar) when using thermodynamic data set 1 (thermodynamic data set 2: Si ~ 6.7 at stage I shown in Figure 8b). Mg-rich staurolite, occurring in polyphase inclusions together with this amphibole in cores of garnet in 18Slo35a, might also suggest that Gt1 inclusion minerals (amphibole, kyanite, staurolite and (clino)zoisite) grew during amphibolite–facies conditions before stage I (Figure 7). From the range of the amphibolite–facies to the determined pressure peak at stage I, nearly isothermal burial or burial at slightly rising temperatures is likely based on the virtually lacking chemical zonation in garnet of both rocks studied. This phenomenon, common in eclogite, was explained by Massonne and Li (2020) by initial formation of garnet after significant overstepping of the P–T limit of this mineral (see Spear, 2017; Spear et al., 2014). Weak garnet zoning was also reported for the Pohorje eclogites studied by Miller, Mundil, et al. (2005) so that it is possible that all Pohorje eclogites (and similar metabasites) had formed along P–T paths from amphibolite– to eclogite–facies conditions.

The P–T conditions at stage II must have been similar to those estimated for stage I because the major element Gt2 composition is similar to that of Gt1. Thus, an effective bulk rock composition, obtained by subtracting the garnet core only, will not change the P–T result for stage II except that the modal content of garnet will be lower by the subtracted amount of garnet. The slight compositional difference between Gt1 and Gt2 (except Cr) could mean that stage II occurred at somewhat higher pressure and lower temperature conditions compared to stage I (Figure 9). However, the oxidation state (Fe^{3+} content) can have a significant influence on the P–T conditions derived for eclogite (e.g., Petrie et al., 2016). Thus, the P–T conditions of stages I and II could differ because the oxidation states at these stages were different. However, our pseudosection calculations for the two bulk rock compositions of 18Slo35a (oxidized and Fe^{3+} free, Table 4) demonstrate that the obtained difference in the P–T conditions is minor (about 30°C at the same pressure; compare Figures 7 and 9) based on stage I results.

The P–T conditions of stages I and II, obtained by using thermodynamic data set 1, are identical within error to those reported by Miller and Konzett (2005), Miller, Mundil, et al. (2005) and Sassi et al. (2004). These authors used the Si content of phengite for geothermobarometry, which was not possible in this study because of the lack of phengite in samples 16Slo1 and 18Slo35a. Thus, we think that the P–T conditions derived by applying thermodynamic data set 2 (16.5 ± 1.5 kbar at 720 ± 20°C for metamorphic stage I of 18Slo35a, Figure 8) are less reliable than those obtained with thermodynamic data set 1. This opinion is also supported by the calculated Si contents in amphibole which are significantly lower (around 6.7 Si pfu) than observed in the core of large amphibole crystals (around 7 Si pfu, Tables 1 and 3). Furthermore, a comparison of P–T results for Variscan eclogite from France, obtained by using either thermodynamic data set 1 or 2, favoured thermodynamic data set 1 as well (Massonne & Li, 2022).

The repeated determination of P–T conditions of 22 ± 4 kbar around 700°C (this study; Miller & Konzett, 2005; Miller, Mundil, et al., 2005; Sassi et al., 2004) for eclogite from the Pohorje Mountains (and the Saualpe-Koralpe area, see, e.g., Miladinova et al., 2021; Schorn et al., 2021) does not exclude the attainment of UHP conditions in this region. However, the geothermobarometric method by Krogh Ravna and Terry (2004) that led to the suggestion of UHP conditions for the Pohorje eclogites seems to overestimate both pressure and temperature. This overestimation was, for example, demonstrated by Hauzenberger et al. (2016); see their Figure 11), who compared different geothermobarometric methods applied to kyanite eclogite PM22 from the Pohorje Mountains. In any case, the assumption that the Pohorje nappe, at least its exposed south-eastern part, represents a coherent UHP terrane (Janák et al., 2004, 2006; Janák, Froitzheim, et al., 2015; Kirst et al., 2010; Sandmann et al., 2016) is inconsistent with the available data.

5.3 | Benefit of varying chromium contents in minerals

The bimodal distribution of Cr across many minerals allows two different metamorphic assemblages to be distinguished. For example, the assemblage of relatively low-Cr minerals occurs in both studied rocks and contains garnet (Gt1), kyanite, staurolite, amphibole and (clino)zoisite in 18Slo35a, but no omphacite was found as

in sample 16Slo1. This low-Cr mineral assemblage preceded the assemblage of Cr-rich minerals.

The garnet Cr (and Ca) X-ray maps allowed discrimination between Gt1 and Gt2 domains, particularly in sample 18Slo35a, where sharp boundaries were discernible in Cr concentrations (Figure 4, the same boundaries in Ca maps were already somewhat blurred). The Gt1-Gt2 boundary was not visible in Mg and Fe maps. Minor intracrystalline cation diffusion of Mg, Fe and to a lesser extent Ca possibly occurred at temperatures above 700°C. Intracrystalline Cr diffusion in garnet appears to be negligible, an observation compatible with previous studies (e.g., Massonne & O'Brien, 2003, see section Introduction).

Two pieces of evidence suggest two separate garnet growth phases separated by a phase of dissolution rather than a continuous metamorphic evolution of eclogite as previously proposed (e.g., Hauzenberger et al., 2016; Janák et al., 2004; Miller & Konzett, 2005; Sassi et al., 2004). The thermodynamic modelling and calculated peak P–T conditions for a single metamorphic burial-exhumation loop result in a minimum modal proportion of 16 vol.% garnet in sample 18Slo35a (see 'oxidized conditions' in Table S5). Instead, we observed a significantly lower proportion (5 vol.% in Table S2). Furthermore, the shape of Gt1, discernible in the Ca and Cr maps of Figure 4, is clearly irregular. We interpret these findings as the result of significant corrosion of Gt1 (Figure 11). Decomposition of Gt1 leading to relics with only 5 vol.% in the rock requires retrogression by significant temperature and/or pressure decrease after stage I (see Figure 7c). As we know from retrogressed eclogite, common decomposition products of garnet are amphibole (+ plagioclase) and/or chlorite often leaving, due to incomplete reaction, garnet relics behind especially at limited influx of H_2O. However, this influx is necessary to form the invoked H_2O-bearing breakdown products during retrogression.

The enrichment in Cr of Gt2 and other minerals requires consideration and explanation. The bulk rock compositions of 16Slo1 and 18Slo35a (Table 4) are compatible with the existence of Cr-rich spinel (chromite) in the protolith (e.g., Miller et al., 2007). We suggest that chromite relics remained at stage I, protected against (further) decomposition by a reaction rim as reported by Hauzenberger et al. (2016) from an eclogite from the Pohorje Mountains. Thus, most Cr in the rock was stored in chromite and, thus, not available for the development of the low-Cr mineral assemblage at stage I (Figure 11). Although chromite is now absent in the studied rocks, there is a significant difference in Cr concentration between Gt1 and Gt2 (Table S2), which can be taken as indirect evidence for its presence before stage II. The proposed dehydration of breakdown minerals (amphibole, chlorite) of Gt1 at rising P–T conditions towards stage II could have been accompanied by deformation leading to oriented clinopyroxene, (clino)zoisite, and amphibole, which are relatively rich in Cr. Thus, the complete breakdown of the proposed chromite relics could have been caused by both deformation and the release of hydrous fluid.

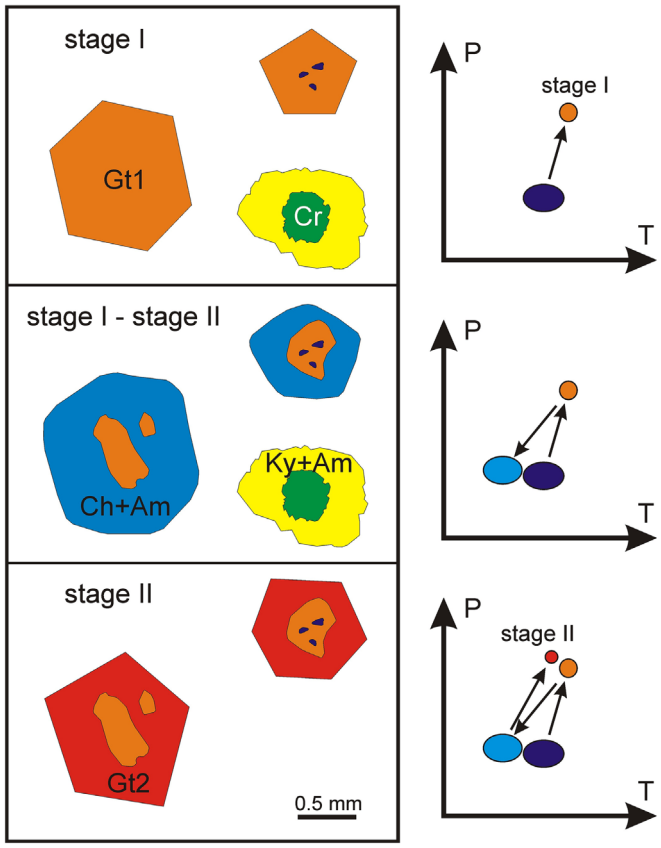

FIGURE 11 Sketch showing the principle P–T evolution (on the right-hand side) towards stage I, to an intermediate stage between stages I and II, and further towards stage II. The postulated changes of garnet and chromite at these stages by mineral reactions (see text) are shown on the left-hand side. Abbreviations as in Figure 7 and Cr, chromite.

An alternative option includes an externally derived Cr-rich fluid from, for instance, nearby ultrabasic rocks (see the serpentinite body in Figure 1c), as suggested by Spandler et al. (2011) and Angiboust et al. (2014). These authors observed an oscillatory zonation of Cr in garnet and suggested pulses of fluid infiltration during garnet growth. We observed a similar zonation but only in garnet of sample 16Slo1. However, further evidence for the transport of Cr over longer distances, such as fluid pathways in the rock wall from which sample 18Slo35a was taken (see section 2.2), is lacking.

Finally, in order to support our hypothesis that Cr-bearing minerals formed at the expense of Cr-rich spinel (chromite) relics in the studied sample, we explored the pressure limits of stable Cr-rich spinel in metabasite compositions similar to that of 18Slo35a. The pseudosection calculations (Section 4.4.3) demonstrate that high Cr contents in the bulk rock combined with oxidizing conditions can lead to an upper pressure limit of chromite in the bulk rock close to the P–T conditions of stages I and II. Although the Cr_2O_3 contents (1–4 wt%) in the bulk rock compositions used for the calculations (Table S2) are significantly higher than in sample 18Slo35a (0.24 wt% Cr_2O_3), local concentrations in the vicinity of chromite may be much higher than in other portions of the rock.

5.4 | Geotectonic consideration

A geotectonic scenario can be developed based on the HP formation of Gt1 (stage I), the subsequent retrogression, and the formation of Cr-rich Gt2 (stage II) outlined in the previous sections. In principle, it is possible that the studied rocks reached near-surface P–T conditions after stage I and before stage II (Figure 11). Subsequently, the formation of Gt2 also required high P–T conditions, which were similar to those that had led to Gt1. As a result, the former breakdown products dehydrated and, thus, caused a re-equilibration at eclogite-facies conditions due to the released H_2O. H_2O excess conditions might have prevailed for a longer period of time. This assumption is supported by large amphibole crystals with lower Si contents at the rim than in the core. Amphibole with lower Si contents crystallized at lower pressures at the expense of clinopyroxene, according to the thermodynamic modelling results, and, thus, along an early exhumation path. The persistence of H_2O-rich fluids during stage II also caused the formation of relatively high Cr concentrations in Gt2 either by dissolution of chromite relics in the metabasites, an explanation which we prefer, or by fluid transport of Cr from the nearby ultrabasic body.

The schematic P–T trajectory shown in Figure 11 is similar to the one derived by Li, Massonne, Koller, and Zhang (2021) for eclogite-hosting micaschist of the Pohorje Mountains. That study suggested a Late Cretaceous HP event around 16 kbar followed by exhumation and cooling. Increasing P–T conditions then led to a second HP event at pressures of 18.5–23 kbar. These pressures are compatible with the stage II conditions determined here for eclogite (and similar metabasite). Li, Massonne, Koller, and Zhang (2021) estimated lower stage II temperatures (around 580°C) than calculated here. They relate the second event to Palaeogene HP metamorphism that is known for regions of the Eastern Alps especially in and around the Tauern window (e.g., Thöni, 2006). The similarities from these terranes support a similar Late Cretaceous and Palaeogene HP evolution in the Pohorje Mountains (Li et al., 2023).

Recent Lu–Hf dating of garnet in Pohorje eclogite has only produced Late Cretaceous ages (Thöni et al., 2008; Sandmann et al., 2016—see also Miladinova et al., 2021, for the Koralpe–Saualpe area). This may be explained by the strong concentration of Lu in garnet cores (here identified as Gt1) and very little in the rims (here identified as Gt2). The age is therefore almost completely weighted to the timing of Gt1 growth.

6 | CONCLUSIONS

The studied HP metabasites from the southern flank of the Pohorje Mountains contain elevated contents of Cr compared to common eclogites (e.g., Miller, Thöni, et al., 2005). The distribution of this element in minerals (Tables 1 and 3) particularly in garnet (Figure 4) allowed two parageneses of minerals characterized by their differing Cr concentrations to be distinguished, especially in metabasite 18Slo35a. The corresponding garnet domains, Cr-poor Gt1 and Cr-rich Gt2, formed at similar P–T conditions of 22.5 ± 2 kbar at 710 ± 25°C (Gt1) and 23 ± 2 kbar at 700 ± 25°C (Gt2) based on thermodynamic data set 1, which we prefer, or around 17 kbar and 710°C (Gt1 and Gt2, thermodynamic data set 2). Stages I and II were separated by partial breakdown of Gt1, which was clearly discernible in Cr X-ray maps. This breakdown should have led to the formation of hydrous minerals as the result of decreasing P–T conditions and influx of H_2O being typical for retrogression. We ascribe the formation of Gt2 during a second HP event, separated in time from the first one, facilitated by the breakdown of the retrograde minerals, formed after stage 1 and assumed relics of Cr-rich spinel (Figure 11). The breakdown of this spinel explains why other minor and trace elements in garnet (e.g., V and Y; see Table S2) do not reflect the formation of Gt2 in the studied metabasites. The derivation of a polycyclic HP metamorphism of these rocks supports the finding by Li, Massonne, Koller, and Zhang (2021) that both Late Cretaceous and Palaeogene orogenic events affected the south-easternmost part of the Eastern Alps.

ACKNOWLEDGEMENTS

We acknowledge the support of Thomas Theye (Universität Stuttgart, Germany) for EMP work, Xiangfa Wang (China University of Geosciences, Wuhan) for SEM

work, Tao Luo and Mufei Li (China University of Geosciences, Wuhan) for LA-ICP-MS analysis and Joachim Opitz (Universität Stuttgart, Germany) for bulk rock analyses with LA-ICP-MS. Friedrich Koller (Geozentrum, Universität Wien) helped us to conduct the field campaigns in the Pohorje Mountains. This work was financially supported by the National Natural Science Foundation of China (No. 42002068), the MOST Special Fund from the State Key Laboratory of GPMR China University of Geosciences (Wuhan), and the 111 Project (BP0719022). The comments by two reviewers (Victor Guevara, Amherst and an anonymous reviewer) helped us to improve an earlier version of the manuscript. The manuscript benefited from the editorial handling by Clare Warren. Open Access funding enabled and organized by Projekt DEAL.

ORCID

Botao Li https://orcid.org/0000-0003-4851-8928
Hans-Joachim Massonne https://orcid.org/0000-0002-2826-4767

REFERENCES

Altherr, R., Lugovic, B., Meyer, H. -P., & Majer, V. (1995). Early Miocene post-collisional calc–alkaline–magmatism along the easternmost segment of the Periadriatic fault system (Slovenia and Croatia). *Mineralogy and Petrology*, *54*, 225–247. https://doi.org/10.1007/BF01162863

Angiboust, S., Pettke, T., de Hoog, J. C. M., Caron, B., & Omcken, O. (2014). Channelized fluid flow and eclogite–facies metasomatism along the subduction shear zone. *Journal of Petrology*, *55*, 883–916. https://doi.org/10.1093/petrology/egu010

Boynton, W. V. (1984). Geochemistry of the rare earth elements: Meteorite studies. In P. Hendersen (Ed.), *Rare earth element geochemistry* (pp. 63–114). Elsevier. https://doi.org/10.1016/B978-0-444-42148-7.50008-3

Brandelik, A. (2009). CALCMIN—An EXCEL™ Visual Basic application for calculating mineral structural formulae from electron microprobe analyses. *Computers & Geosciences*, *35*, 1540–1551. https://doi.org/10.1016/j.cageo.2008.09.011

Bruand, E., Stüwe, K., & Proyer, A. (2010). Pseudosection modelling for a selected eclogite body from the Koralpe (Hohl), Eastern Alps. *Mineralogy and Petrology*, *99*, 75–87. https://doi.org/10.1007/s00710-009-0097-7

Caddick, M., Konopasek, J., & Thompson, A. B. (2010). Preservation of garnet growth zoning and the duration of prograde metamorphism. *Journal of Petrology*, *51*, 2327–2347. https://doi.org/10.1093/petrology/egq059

Carlson, W. D. (2006). Rates of Fe, Mg, Mn, and Ca diffusion in garnet. *American Mineralogist*, *91*, 1–11. https://doi.org/10.2138/am.2006.2043

Carlson, W. D. (2012). Rates and mechanism of Y, REE, and Cr diffusion in garnet. *American Mineralogist*, *97*, 1598–1618. https://doi.org/10.2138/am.2012.4108

Carlson, W. D., & Schwarze, E. (1997). Petrological significance of prograde homogenization of growth zoning in garnet: An example from the llano uplift. *Journal of Metamorphic Geology*, *15*, 631–644. https://doi.org/10.1111/j.1525-1314.1997.tb00640.x

Chakraborty, S., & Ganguly, J. (1991). Compositional zoning and cation diffusion in garnets. *Advances in Physical Geochemistry*, *8*, 121–175. https://doi.org/10.1007/978-1-4613-9019-0_4

Chang, R., Neubauer, F., Liu, Y., Genser, J., Jin, W., Yuan, S., Guan, Q., Huang, Q., & Li, W. (2020). Subduction of a rifted passive continental margin: The Pohorje case of Eastern Alps–constraints from geochronology and geochemistry. *Swiss Journal of Geosciences*, *113*, 14. https://doi.org/10.1186/s00015-020-00369-z

Connolly, J. A. D. (2005). Computation of phase equilibria by linear programming: A tool for geodynamic modeling and its application to subduction zone decarbonation. *Earth and Planetary Science Letters*, *236*, 524–541. https://doi.org/10.1016/j.epsl.2005.04.033

Dachs, E., & Proyer, A. (2002). Constraints on the duration of high-pressure metamorphism in the Tauern Window from diffusion modelling of discontinuous growth zones in eclogite garnet. *Journal of Metamorphic Geology*, *20*, 769–780. https://doi.org/10.1046/j.1525-1314.2002.00404.x

Dal Piaz, G. V., Bistacchi, A., & Massironi, M. (2003). Geological outline of the Alps. *Episodes*, *26*, 175–180. https://doi.org/10.18814/epiiugs/2003/v26i3/004

Faryad, S. W., & Hoinkes, G. (2003). P-T gradient of Eo-Alpine metamorphism within the Austroalpine basement units east of the Tauern Window (Austria). *Mineralogy and Petrology*, *77*, 129–159. https://doi.org/10.1007/s00710-002-0196-1

Fodor, L. I., Gerdes, A., Dunkl, I., Koroknai, B., Pécskay, Z., Trajanova, M., Horváth, P., Vrabec, M., Jelen, B., Balogh, K., & Frisch, W. (2008). Miocene emplacement and rapid cooling of the Pohorje pluton at the Alpine–Pannonian–Dinaridic junction, Slovenia. *Swiss Journal of Geosciences*, *101*, 255–271. https://doi.org/10.1007/s00015-008-1286-9

Fuhrman, M. L., & Lindsley, D. H. (1988). Ternary-feldspar modeling and thermometry. *American Mineralogist*, *73*, 201–215.

George, F. R., Gaidies, F., & Boucher, B. (2018). Population-wide garnet growth zoning revealed by LA-ICP-MS mapping: Implications for trace element equilibration and syn-kinematic deformation during crystallisation. *Contributions to Mineralogy and Petrology*, *173*, 74. https://doi.org/10.1007/s00410-018-1503-0

Habler, G., & Thöni, M. (2001). Preservation of Permo-Triassic low-pressure assemblages in the Cretaceous high-pressure metamorphic Saualpe crystalline basement (Eastern Alps, Austria). *Journal of Metamorphic Geology*, *19*, 679–697. https://doi.org/10.1046/j.0263-4929.2001.00338.x

Hauke, M., Froitzheim, N., Nagel, T. J., Miladinova, I., Fassmer, K., Fonseca, R. O. C., Sprung, P., & Münker, C. (2019). Two high-pressure metamorphic events, Variscan and Alpine, dated by Lu–Hf in an eclogite complex of the Austroalpine nappes (Schobergruppe, Austria). *International Journal of Earth Sciences*, *108*, 1317–1331. https://doi.org/10.1007/s00531-019-01708-8

Hauzenberger, C. A., Taferner, H., & Konzett, J. (2016). Genesis of chromium-rich kyanite in eclogite-facies Cr-spinel-bearing gabbroic cumulates, Pohorje Massif, Eastern Alps. *American Mineralogist*, *101*, 448–460. https://doi.org/10.2138/am-2016-5178

Herg, A., & Stüwe, K. (2018). Tectonic interpretation of the metamorphic field gradient south of the Koralpe in the Eastern

Alps. *Austrian Journal of Earth Sciences*, *111*(2), 155–170. https://doi.org/10.17738/ajes.2018.0010

Heritsch, H. (1973). Die Bildungsbedingungen von alpinotypem Eklogitamphibolit und Metagabbro, erläutert an Gesteinen der Koralpe, Steiermark. *Tschermaks Mineralogische Und Petrographische Mitteilungen*, *19*, 213–271. https://doi.org/10.1007/BF01087045

Hoinkes, G., Koller, F., Rantitsch, G., Dachs, E., Höck, V., Neubauer, F., & Schuster, R. (1999). Alpine metamorphism of the Eastern Alps. *Schweizerische Mineralogische und Petrographische Mitteilungen*, *79*, 155–181.

Holland, T. J. B. (1979). High water activities in the generation of high pressure kyanite eclogites of the Tauern Window, Austria. *The Journal of Geology*, *87*, 1–27. https://doi.org/10.1086/628388

Holland, T. J. B., & Powell, R. (1998). An internally consistent thermodynamic data set for phases of petrological interest. *Journal of Metamorphic Geology*, *16*, 309–343. https://doi.org/10.1111/j.1525-1314.1998.00140.x

Holland, T. J. B., & Powell, R. (2011). An improved and extended internally-consistent thermodynamic dataset for phases of petrological interest, involving a new equation of state for solids. *Journal of Metamorphic Geology*, *29*, 333–383. https://doi.org/10.1111/j.1525-1314.2010.00923.x

Hoschek, G. (2004). Comparison of calculated P-T pseudosections for a kyanite eclogite from the Tauern Window, eastern Alps, Austria. *European Journal of Mineralogy*, *16*, 59–72. https://doi.org/10.1127/0935-1221/2004/0016-0059

Hoschek, G., Konzett, J., & Tessadri, R. (2010). Phase equilibria in quartzitic garnet-kyanite-chloritoid micaschist from the Eclogite Zone, Tauern Window, Eastern Alps. *European Journal of Mineralogy*, *22*, 721–732. https://doi.org/10.1127/0935-1221/2010/0022-2049

Hurai, V., Janák, M., & Thomas, R. (2010). Fluid-assisted retrogression of garnet and P–T history of metapelites from HP/UHP metamorphic terrane (Pohorje Mountains, Eastern Alps). *Contributions to Mineralogy and Petrology*, *160*, 203–218. https://doi.org/10.1007/s00410-009-0473-7

Ippen, J. A. (1893). Zur Kenntniss der Eklogite und Amphibolitgesteine des Bachergebirges. *Mittheilungen des naturwissenschaftlichen Vereines für Steiermark*, *1892*, 328–369.

Janák, M., Cornell, D., Froitzheim, N., De Hoog, J. C., Broska, I., Vrabec, M., & Hurai, V. (2009). Eclogite-hosting metapelites from the Pohorje Mountains (Eastern Alps): P-T evolution, zircon geochronology and tectonic implications. *European Journal of Mineralogy*, *21*, 1191–1212. https://doi.org/10.1127/0935-1221/2009/0021-1966

Janák, M., Froitzheim, N., Lupták, B., Vrabec, M., & Ravna, E. J. K. (2004). First evidence for ultrahigh-pressure metamorphism of eclogites in Pohorje, Slovenia: Tracing deep continental subduction in the eastern Alps. *Tectonics*, *23*, TC5014. https://doi.org/10.1029/2004TC001641

Janák, M., Froitzheim, N., Vrabec, M., Krogh Ravna, E. J., & De Hoog, J. C. M. (2006). Ultrahigh-pressure metamorphism and exhumation of garnet peridotite in Pohorje, Eastern Alps. *Journal of Metamorphic Geology*, *24*, 19–31. https://doi.org/10.1111/j.1525-1314.2005.00619.x

Janák, M., Froitzheim, N., Yoshida, K., Sasinková, V., Nosko, M., Kobayashi, T., Hirajima, T., & Vrabec, M. (2015). Diamond in metasedimentary crustal rocks from Pohorje, Eastern Alps: A window to deep continental subduction. *Journal of Metamorphic Geology*, *33*, 495–512. https://doi.org/10.1111/jmg.12130

Janák, M., Uher, P., Krogh Ravna, E., Kullerud, K., & Vrabec, M. (2015). Chromium-rich kyanite, magnesiostaurolite and corundum in ultrahigh-pressure eclogites (examples from Pohorje Mountains, Slovenia and Tromsø Nappe, Norway). *European Journal of Mineralogy*, *27*, 377–392. https://doi.org/10.1127/ejm/2015/0027-2436

Jennings, E. S., & Holland, T. J. B. (2015). A simple thermodynamic model for melting of peridotite in the system NCFMASOCr. *Journal of Petrology*, *56*, 869–892. https://doi.org/10.1093/petrology/egv020

Jiang, J., & Lasaga, A. C. (1990). The effect of post-growth thermal events on growth-zoned garnet: Implications for metamorphic P-T history calculations. *Contributions to Mineralogy and Petrology*, *105*, 454–459. https://doi.org/10.1007/BF00286832

Kirst, F., Sandmann, S., Nagel, T., Froitzheim, N., & Janák, M. (2010). Tectonic evolution of the southeastern part of the Pohorje Mountains (Eastern Alps, Slovenia). *Geologica Carpathica*, *61*, 451–461. https://doi.org/10.2478/v10096-010-0027-y

Krenn, E., Janák, M., Finger, F., Broska, I., & Konečný, P. (2009). Two types of metamorphic monazite with contrasting La/Nd, Th, and Y signatures in an ultrahigh-pressure metapelite from the Pohorje Mountains, Slovenia: Indications for pressure-dependent REE exchange between apatite and monazite? *American Mineralogist*, *94*, 801–815. https://doi.org/10.2138/am.2009.2981

Krogh Ravna, E. J., & Terry, P. (2004). Geothermobarometry of UHP and HP eclogites and schists—An evaluation of equilibria among garnet-clinopyroxene-kyanite-phengite-coesite/-quartz. *Journal of Metamorphic Geology*, *22*, 579–592. https://doi.org/10.1111/j.1525-1314.2004.00534.x

Li, B., Ge, J., & Zhang, B. (2018). Diffusion in garnet: A review. *Acta Geochemica*, *37*, 19–31. https://doi.org/10.1007/s11631-017-0187-x

Li, Z., Hu, Z. C., Liu, Y. S., Gao, S., Li, M., Zong, K. Q., Chen, H. H., & Hu, S. H. (2015). Accurate determination of elements in silicate glass by nanosecond and femtosecond laser ablation ICP-MS at high spatial resolution. *Chemical Geology*, *400*, 11–23. https://doi.org/10.1016/j.chemgeo.2015.02.004

Li, B., Massonne, H.-J., Hartmann, L. A., Zhang, J., & Luo, T. (2021). Kyanite-garnet granulite from the Andrelândia nappe system, Brasília belt, registers two late Neoproterozoic metamorphic cycles. *Precambrian Research*, *355*, 106086. https://doi.org/10.1016/j.precamres.2020.106086

Li, B., Massonne, H.-J., Koller, F., & Zhang, J.-F. (2021). Metapelite from the high-ultrahigh pressure terrane of the Eastern Alps (Pohorje Mountains, Slovenia)—New pressure, temperature, and time constraints on a polymetamorphic rock. *Journal of Metamorphic Geology*, *39*, 695–726. https://doi.org/10.1111/jmg.12581

Li, B., Massonne, H.-J., & Opitz, J. (2017). Clockwise and anticlockwise P-T paths of high-pressure rocks from the 'La Pioza' eclogite body of the Malpica-Tuy zone, NW Spain. *Journal of Petrology*, *58*, 1363–1392. https://doi.org/10.1093/petrology/egx057

Li, B., Massonne, H.-J., & Yuan, X. (2023). Wealth of P-T-t information from metasediments in the HP-UHP terrane of the Pohorje Mountains, Slovenia, elucidates the evolution of the Eastern Alps. *Journal of Metamorphic Geology*, in press. https://doi.org/10.1111/jmg.12740

Liu, Y. S., Hu, Z. C., Gao, S., Günther, D., Xu, J., Gao, C. G., & Chen, H. H. (2008). In situ analysis of major and trace elements of anhydrous minerals by LA-ICP-MS without applying an internal standard. *Chemical Geology*, *257*, 34–43. https://doi.org/10.1016/j.chemgeo.2008.08.004

Luo, T., Hu, Z. C., Zhang, W., Günther, D., Liu, Y. S., Zong, K. Q., & Hu, S. H. (2018). Reassessment of the influence of carrier gases He and Ar on signal intensities in 193 nm excimer LA-ICP-MS analysis. *Journal of Analytical Atomic Spectrometry*, *33*, 1655–1663.

Martin, A. J. (2009). Sub-millimeter heterogeneity of yttrium and chromium during growth of semi-pelitic garnet. *Journal of Petrology*, *50*, 1713–1727. https://doi.org/10.1093/petrology/egp050

Massonne, H.-J. (2012). Formation of amphibole and clinozoisite–epidote in eclogite owing to fluid infiltration during exhumation in a subduction channel. *Journal of Petrology*, *53*, 1969–1998. https://doi.org/10.1093/petrology/egs040

Massonne, H.-J. (2013). Constructing the pressure–temperature path of ultrahigh-pressure rocks. *Elements*, *9*, 267–272. https://doi.org/10.2113/gselements.9.4.267

Massonne, H.-J., & Li, B. (2020). Zoning of eclogitic garnet cores—A key pattern demonstrating the dominance of tectonic erosion as part of the burial process of worldwide occurring eclogites. *Earth-Science Reviews*, *210*, 103356. https://doi.org/10.1016/j.earscirev.2020.103356

Massonne, H.-J., & Li, B. (2022). Eclogite with unusual atoll garnet from the southern Armorican Massif, France: Pressure-temperature path and geodynamic implications. *Tectonophysics*, *823*, 229183. https://doi.org/10.1016/j.tecto.2021.229183

Massonne, H.-J., & O'Brien, P. J. (2003). The Bohemian Massif and the NW Himalaya. In D. A. Carswell & R. Compagnoni (Eds.), *Ultrahigh pressure metamorphism* (Vol. 5, pp. 145–187). European Mineralogical Union Notes in Mineralogy. https://doi.org/10.1180/EMU-notes.5.6

Massonne, H.-J., Opitz, J., & van Staal, C. (2022). Geochemical and petrographic characteristics of eclogite–amphibolite bodies in the northern Fleur-de-Lys Supergroup of NE Newfoundland. *Journal of Mineralogy and Geochemistry (Former Neues Jahrbuch für Mineralogie Abhandlungen)*, *198*, 1–23. https://doi.org/10.1127/njma/2022/0315

McDonough, W. F., & Sun, S. S. (1995). The composition of the Earth. *Chemical Geology*, *120*, 223–253. https://doi.org/10.1016/0009-2541(94)00140-4

Miladinova, I., Froitzheim, N., Nagel, T. J., Janák, M., Fonseca, R. O. C., Sprung, P., & Münker, C. (2021). Constraining the process of intracontinental subduction in the Austroalpine Nappes: Implications from petrology and Lu–Hf geochronology of eclogites. *Journal of Metamorphic Geology*, *40*(3), 423–456. https://doi.org/10.1111/jmg.12634

Miller, C. (1990). Petrology of the type locality eclogites from the Koralpe and Saualpe (Eastern Alps), Austria. *Schweizerische Mineralogische und Petrographische Mitteilungen*, *70*, 287–300.

Miller, C., & Konzett, J. (2005). Comment on "first evidence for ultrahigh-pressure metamorphism of eclogites in Pohorje, Slovenia: Tracing deep continental subduction in the eastern Alps" by Marian Janák et al. *Tectonics*, *24*, TC6010. https://doi.org/10.1029/2004TC001765

Miller, C., Mundil, R., Thöni, M., & Konzett, J. (2005). Refining the timing of eclogite metamorphism: A geochemical, petrological, Sm–Nd and U–Pb case study from the Pohorje Mountains, Slovenia (eastern Alps). *Contributions to Mineralogy and Petrology*, *150*, 70–84. https://doi.org/10.1007/s00410-005-0004-0

Miller, C., Stosch, H. G., & Hoernes, S. (1988). Geochemistry and origin of eclogites from the type locality Koralpe and Saualpe, Eastern Alps, Austria. *Chemical Geology*, *67*, 103–118. https://doi.org/10.1016/0009-2541(88)90009-5

Miller, C., & Thöni, M. (1997). Eo-Alpine eclogitisation of Permian MORB-type gabbros in the Koralpe (Eastern Alps, Austria): New geochronological, geochemical and petrological data. *Chemical Geology*, *137*, 283–310. https://doi.org/10.1016/S0009-2541(96)00165-9

Miller, C., Thöni, M., Konzett, J., Kurz, W., & Schuster, R. (2005). Eclogites from the Koralpe and Saualpe type-localities, Eastern Alps, Austria. *Mitteilungen der Österreichischen Mineralogischen Gesellschaft*, *150*, 227–263.

Miller, C., Zanetti, A., Thöni, M., & Konzett, J. (2007). Eclogitisation of gabbroic rocks. Redistribution of trace elements and Zr in rutile thermometry in an Eo-Alpine subduction zone (Eastern Alps). *Chemical Geology*, *239*, 96–123. https://doi.org/10.1016/j.chemgeo.2007.01.001

Neubauer, F., Genser, J., & Handler, R. (2000). The Eastern Alps: Result of a two-stage collision process. *Mitteilungen der Österreichischen Geologischen Gesellschaft*, *92*, 117–134.

Pan, R., Macris, C. A., & Menold, C. A. (2020). Thermodynamic modeling of high-grade metabasites: A case study using the Tso Morari UHP eclogite. *Contributions to Mineralogy and Petrology*, *175*, 78. https://doi.org/10.1007/s00410-020-01717-w

Perchuk, A. L., Burchard, M., Schertl, H. -P., Maresch, W. V., Gerya, T. V., Bernhard, H. -J., & Vidal, O. (2009). Diffusion of divalent cations in garnet: Multi-couple experiments. *Contributions to Mineralogy and Petrology*, *157*, 573–592. https://doi.org/10.1007/s00410-008-0353-6

Petrie, M. B., Massonne, H.-J., Gilotti, J. A., McClelland, W. C., & van Staal, C. (2016). The P–T path of eclogites in the St. Cyr klippe, Yukon, Canada: Permian metamorphism of a coherent high-pressure unit in an accreted terrane of the North American Cordillera. *European Journal of Mineralogy*, *28*, 1111–1130. https://doi.org/10.1127/ejm/2016/0028-2576

Ratschbacher, L., Frisch, W., Neubauer, F., Schmid, S. M., & Neugebauer, J. (1989). Extension in compressional orogenic belts: The eastern Alps. *Geology*, *17*, 404–407. https://doi.org/10.1130/0091-7613(1989)017<0404:EICOBT>2.3.CO;2

Rubatto, D., Burger, M., Lanari, P., Hattendorf, B., Schwarz, G., Nef, C., Keresztes Schmidt, P., Hermann, J., Vho, A., & Günther, D. (2020). Identifcation of growth mechanisms in metamorphic garnet by high-resolution trace element mapping with LA-ICP-TOFMS. *Contributions to Mineralogy and Petrology*, *175*, 61. https://doi.org/10.1007/s00410-020-01700-5

Sandmann, S., Herwartz, D., Kirst, F., Froitzheim, N., Nagel, T. J., Fonseca, R. O. C., Münker, C., & Janák, M. (2016). Timing of eclogite–facies metamorphism of mafic and ultramafic rocks from the Pohorje Mountains (Eastern Alps, Slovenia) based on

Lu–Hf garnet geochronometry. *Lithos*, *262*, 576–585. https://doi.org/10.1016/j.lithos.2016.08.002

Sassi, R., Mazzoli, C., Miller, C., & Konzett, J. (2004). Geochemistry and metamorphic evolution of the Pohorje Mountain eclogites from the easternmost Austroalpine basement of the Eastern Alps (Northern Slovenia). *Lithos*, *78*, 235–261. https://doi.org/10.1016/j.lithos.2004.05.002

Schmid, S. M., Fügenschuh, B., Kissling, E., & Schuster, R. (2004). Tectonic map and overall architecture of the Alpine orogeny. *Eclogae Geologicae Helvetiae*, *97*, 93–117. https://doi.org/10.1007/s00015-004-1113-x

Schorn, S., Hartnady, M. I. H., Diener, J. F. A., Clark, C., & Harris, C. (2021). H_2O-fluxed melting of eclogite during exhumation: An example from the eclogite type-locality, Eastern Alps (Austria). *Lithos*, *390-391*, 106118. https://doi.org/10.1016/j.lithos.2021.106118

Schorn, S., & Stüwe, K. (2016). The Plankogel detachment of the Eastern Alps: Petrological evidence for an orogen-scale extraction fault. *Journal of Metamorphic Geology*, *34*, 147–166. https://doi.org/10.1111/jmg.12176

Schulz, B. (2017). Polymetamorphism in garnet micaschists of the Saualpe Eclogite Unit (Eastern Alps, Austria), resolved by automated SEM methods and EMP–Th–U–Pb monazite dating. *Journal of Metamorphic Geology*, *35*, 141–163. https://doi.org/10.1111/jmg.12224

Schuster, R., & Stüwe, K. (2008). Permian metamorphic event in the Alps. *Geology*, *36*, 603–606. https://doi.org/10.1130/G24703A.1

Spandler, C., Pettke, T., & Rubatto, D. (2011). Internal and external fluid sources for eclogite–facies veins in the Monviso metaophiolite, Western Alps: Implications for fluid flow in subduction zones. *Journal of Petrology*, *52*, 1207–1236. https://doi.org/10.1093/petrology/egr025

Spear, F. S. (2017). Garnet growth after overstepping. *Chemical Geology*, *466*, 491–499. https://doi.org/10.1016/j.chemgeo.2017.06.038

Spear, F. S., & Franz, G. (1986). P-T evolution of metasediments from the Eclogite Zone, south-central Tauern Window, Austria. *Lithos*, *19*, 219–234. https://doi.org/10.1016/0024-4937(86)90024-1

Spear, F. S., & Kohn, M. J. (1996). Trace element zoning in garnet as a monitor of crustal melting. *Geology*, *24*, 1099–1102. https://doi.org/10.1130/0091-7613(1996)024<1099:TEZIGA>2.3.CO;2

Spear, F. S., Thomas, J. B., & Hallett, B. W. (2014). Overstepping the garnet isograd: A comparison of QuiG barometry and thermodynamic modeling. *Contributions to Mineralogy and Petrology*, *168*(3), 1059. https://doi.org/10.1007/s00410-014-1059-6

Stöckhert, B., Massonne, H.-J., & Nowlan, E. U. (1997). Low differential stress during high-pressure metamorphism: The microstructural record of a metapelite from the Eclogite Zone, Tauern Window, Eastern Alps. *Lithos*, *41*, 103–118. https://doi.org/10.1016/S0024-4937(97)82007-5

Tenczer, V., & Stüwe, K. (2003). The metamorphic field gradient in the eclogite type locality, Koralpe region, Eastern Alps. *Journal of Metamorphic Geology*, *21*, 377–393. https://doi.org/10.1046/j.1525-1314.2003.00448.x

Thöni, M. (2003). Sm–Nd isotope systematics in garnet from different lithologies (Eastern Alps): Age results, and an evaluation of potential problems for garnet Sm–Nd chronometry. *Chemical Geology*, *194*, 353–379. https://doi.org/10.1016/S0009-2541(02)00419-9

Thöni, M. (2006). Dating eclogite-facies metamorphism in the Eastern Alps—Approaches, results, interpretations: A review. *Mineralogy and Petrology*, *88*, 123–148. https://doi.org/10.1007/s00710-006-0153-5

Thöni, M., & Jagoutz, E. (1992). Some new aspects of dating eclogites in orogenic belts: Sm–Nd, Rb–Sr, and Pb–Pb isotopic results from the Austroalpine Saualpe and Koralpe type-locality (Carinthia/Styria, southeastern Austria). *Geochimica et Cosmochimica Acta*, *56*, 347–368. https://doi.org/10.1016/0016-7037(92)90138-9

Thöni, M., & Miller, C. (1996). Garnet Sm–Nd data from the Saualpe and the Koralpe (Eastern Alps, Austria): Chronological and P-T constraints on the thermal and tectonic history. *Journal of Metamorphic Geology*, *14*, 453–466. https://doi.org/10.1046/j.1525-1314.1996.05995.x

Thöni, M., & Miller, C. (2009). The "Permian event" in the Eastern European Alps: Sm–Nd and P–T data recorded by multi-stage garnet from the Plankogel unit. *Chemical Geology*, *260*, 20–36. https://doi.org/10.1016/j.chemgeo.2008.11.017

Thöni, M., & Miller, C. (2010). Andalusite formation in a fast exhuming high-P wedge: Textural, microchemical, and Sm–Nd and Rb–Sr age constraints for a Cretaceous P–T–t path at Kienberg, Saualpe (Eastern Alps). *Austrian Journal of Earth Sciences*, *103*, 118–131.

Thöni, M., Miller, C., Blichert-Toft, J., Whitehouse, M. J., Konzett, J., & Zanetti, A. (2008). Timing of high-pressure metamorphism and exhumation of the eclogite type-locality (Kupplerbrunn–Prickler Halt, Saualpe, south-eastern Austria): Constraints from correlations of the Sm–Nd, Lu–Hf, U–Pb and Rb–Sr isotopic systems. *Journal of Metamorphic Geology*, *26*, 561–581. https://doi.org/10.1111/j.1525-1314.2008.00778.x

Uher, P., Janák, M., Konečný, P., & Vrabec, M. (2014). Rare-element granitic pegmatite of Miocene age emplaced in UHP rocks from Visole, Pohorje Mountains (Eastern Alps, Slovenia): Accessory minerals, monazite and uraninite chemical dating. *Geologica Carpathica*, *65*, 131–146. https://doi.org/10.2478/geoca-2014-0009

Vrabec, M., Janák, M., Froitzheim, N., & De Hoog, J. C. (2012). Phase relations during peak metamorphism and decompression of the UHP kyanite eclogites, Pohorje Mountains (Eastern Alps, Slovenia). *Lithos*, *144*, 40–55. https://doi.org/10.1016/j.lithos.2012.04.004

Yang, P., & Rivers, T. (2001). Chromium and manganese zoning in pelitic garnet and kyanite: Spiral, overprint, and oscillatory (?) zoning patterns and the role of growth rate. *Journal of Metamorphic Geology*, *19*, 455–474. https://doi.org/10.1046/j.0263-4929.2001.00323.x

SUPPORTING INFORMATION

Additional supporting information can be found online in the Supporting Information section at the end of this article.

FIGURE S1. Estimation of the P-T conditions of stage I (ellipsis, assemblage of Cr-poor minerals) considering the amphibole-out curve and relevant parameters for garnet and amphibole of sample 16Slo1.

Table S1. Quality check for our LA-ICP-MS analyses of garnet at Wuhan comparing reference values with mean results of the analysed standards (see also section 3).

Table S2. Calculation table for the estimation of bulk-rock and effective bulk-rock compositions from average mineral compositions (abbreviations as in the text, eff. = effective, norm. = normalized).

Table S3. Trace-element contents in garnet clinopyroxenite 18Slo35a. In addition, the mass numbers of the isotopes used to determine the corresponding element contents by LA-ICP-MS are given.

Table S4. Calculated mineral modes for eclogite 16Slo1 at conditions around the derived pressure peaks using thermodynamic data set 1.

Table S5. Calculated mineral modes for garnet clinopyroxenite 18Slo35a at conditions around the derived pressure peaks using thermodynamic data set 1.

Table S6. Calculated mineral modes for garnet clinopyroxenite 18Slo35a at conditions around the derived pressure peaks using thermodynamic data set 2.

How to cite this article: Li, B., & Massonne, H.-J. (2024). Chromium in minerals as tracer of the polycyclic evolution of eclogite and related metabasite from the Pohorje Mountains, Slovenian Eastern Alps. *Journal of Metamorphic Geology*, *42*(1), 63–88. https://doi.org/10.1111/jmg.12746

APPENDIX A: SOLID SOLUTION MODELS USED

In combination with the older thermodynamic data set by Holland & Powell (1998, updated 2002) we used the following solid-solution models (see file solution_model1.dat in Massonne et al., 2018) for pseudosection calculations: (1) GlTrTsPg for amphibole (e.g., Wei et al., 2003), (2) Carp for carpholite as ideal solid solution based on the thermodynamic data for end-members carpholite and Mg–carpholite given by Holland and Powell (1998), (3) Chl (HP) for chlorite (Holland et al., 1998), (4) Ctd (HP) for chloritoid taken 'from THERMOCALC' (written comm. by J.A.D. Connolly), (5) Ep (HP) for epidote (Holland & Powell, 1998), (6) Gt (HP) for garnet (Holland & Powell, 1998), (7) IlGkPy (maximum 30 mol% geikilite component) as ideal solid solution (see above), (8) Mica(M) for paragonite (Massonne, 2010), (9) Omph (HP) for omphacite (Holland & Powell, 1996; Zeh et al., 2005), (10) Opx (HP) for orthopyroxene (Powell & Holland, 1999), (11) feldspar for plagioclase (Fuhrman & Lindsley, 1988) and (12) St (HP) for staurolite taken 'from THERMOCALC' (written comm. by J.A.D. Connolly). Quartz, magnetite, sapphirine, zoisite, rutile, titanite, Al–silicates, lawsonite and talc were considered as pure phases. Feldspar (ab), amphibole (rieb, mrb, cumm and grun) and melt (h2oL) components, sudoite (sud) and the O_2 buffers qfm and mthm were excluded.

The solid solution models used in combination with the more recent thermodynamic data set by Holland and Powell (2011) were cAmph(G) for amphibole (Green et al., 2016), Chl(W) for chlorite (White et al., 2014), Ep (HP11) for epidote (Holland & Powell, 2011), Gt(W) for garnet (White et al., 2014), Omph (GHP) for omphacite (Green et al., 2007) with Margules parameters updated by Green et al. (2016) and T for talc as ideal solid solution of three components. The solid solution models for ilmenite, paragonite, orthopyroxene and plagioclase were the same as given above. Quartz, rutile, Al-silicates and lawsonite were considered as pure phases. A melt component (h2oL), a chlorite component (f3clin), a feldspar component (ab), zoisite and the O_2 buffers qfm and mthm were excluded.

Additional references:

Green, E. C. R., Holland, T. J. B. & Powell, R. (2007). An order–disorder model for omphacitic pyroxenes in the system jadeite–diopside–hedenbergite–acmite, with applications to eclogite rocks. *American Mineralogist*, 92, 1,181–1,189.

Green, E. C. R., White, R. W., Diener, J. F. A., Powell, R., Holland, T. J. B. & Palin, R. M. (2016). Activity–composition relations for the calculation of partial melting equilibria in metabasic rocks. *Journal of Metamorphic Geology*, 34, 845–869.

Holland, T. & Powell, R. (1996). Thermodynamics of order–disorder in minerals: II. Symmetric formalism applied to solid solutions. *American Mineralogist*, 81, 1,425–1,437.

Holland, T., Baker, J. M. & Powell, R. (1998). Mixing properties and activity–composition relationships of chlorites in the system MgO–FeO–Al_2O_3–SiO_2–H_2O. *European Journal of Mineralogy*, 10, 395–406.

Massonne, H.-J. (2010). Phase relations and dehydration behaviour of calcareous sediments at very-low to low grade metamorphic conditions. *Periodico di Mineralogia*, 79, 21–43.

Massonne, H.-J., Cruciani, G., Franceschelli, M. & Musumeci, G. (2018). Anti-clockwise pressure–temperature paths record Variscan upper-plate exhumation: Example from micaschists of the Porto Vecchio region, Corsica. *Journal of Metamorphic Geology*, 36, 55–77.

Powell, R. & Holland, T. (1999). Relating formulations of the thermodynamics of mineral solid solutions:

Activity modelling of pyroxenes, amphiboles, and micas. *American Mineralogist*, 84, 1–14.

Wei, C. J., Powell, R. & Zhang, L. F. (2003). Eclogites from the south Tianshan, NW China: petrological characteristic and calculated mineral equilibria in the Na_2O-CaO-FeO-MgO-Al_2O_3-SiO_2-H_2O system. *Journal of Metamorphic Geology*, 21, 163–179.

White, R. W., Powell, R., Holland, T. J. B., Johnson, T. E. & Green, E. C. R. (2014). New mineral activity–composition relations for thermodynamic calculations in metapelitic systems. *Journal of Metamorphic Geology*, 32, 261–286.

Zeh, A., Holland, T. J. B. & Klemd, R. (2005). Phase relationships in grunerite–garnet-bearing amphibolites in the system CFMASH, with applications to metamorphic rocks from the Central Zone of the Limpopo Belt, South Africa. *Journal of Metamorphic Geology*, 23, 1–17.